WRPS-67868
Revision 0

Acetonitrile Destruction and Fate of Organics in the Reverse Osmosis System at the ETF

Prepared for the U.S. Department of Energy
Assistant Secretary for Environmental Management

Contractor for the U.S. Department of Energy
Office of River Protection under Contract DE-AC27-08RV14800

P.O. Box 850
Richland, Washington 99352

WRPS-67868
Revision 0

Acetonitrile Destruction and Fate of Organics in the Reverse Osmosis System at the ETF

I. L. Pegg
Vitreous State Laboratory of The Catholic University of America

H. Abramowitz
Vitreous State Laboratory of The Catholic University of America

M. Brandys
Vitreous State Laboratory of The Catholic University of America

N. Mecholsky
Vitreous State Laboratory of The Catholic University of America

D. J. Swanberg
Washington River Protection Solutions

R. S. Skeen
Washington River Protection Solutions

Date Published
December 2021

DOE ORP

Prepared for the U.S. Department of Energy
Assistant Secretary for Environmental Management

Contractor for the U.S. Department of Energy
Office of River Protection under Contract DE-AC27-08RV14800

P.O. Box 850
Richland, Washington 99352

Release Approval Date

VSL-21R5050-1

Final Report

Acetonitrile Destruction and Fate of Organics in the Reverse Osmosis System at the ETF

prepared by

Marek Brandys, Howard Abramowitz, Nicholas Mecholsky, and Ian L. Pegg

Vitreous State Laboratory
The Catholic University of America
Washington, DC 20064

for

Atkins Energy Federal EPC, Inc.
Columbia, MD 21046

and

Washington River Protection *Solutions*, LLC
Richland, WA

November 8, 2021

Rev. 0, 12/20/21

Completeness of Testing:

This report describes the results of work and testing specified by the referenced WRPS approved Test Plan(s). The work and any associated testing followed established quality assurance requirements and were conducted as authorized. The descriptions provided in this test report are an accurate account of both the conduct of the work and the data collected. Results required by the Test Plan are reported. Also reported are any unusual or anomalous occurrences that are different from the starting hypotheses. The test results and this report have been reviewed and verified.

I.L. Pegg: _____ **Date:** 12/21/21
VSL Program Director/Principal Investigator

I. Joseph: Innocent Joseph **Date:** 12-21-21
Atkins Sub-Contract Manager

TABLE OF CONTENTS

List of Tables

List of Figures

List of Abbreviations

ASME	American Society of Mechanical Engineers
CUA	Catholic University of America
DFLAW	Direct Feed Low Activity Waste
DOE	Department of Energy
EMF	Effluent Management Facility
ERDF	Environmental Restoration Disposal Facility
ETF	Effluent Treatment Facility
GC-MS	Gas Chromatography - Mass Spectroscopy
IC	Ion Chromatography
ICP-AES	Inductively Coupled Plasma – Atomic Emission Spectroscopy
IDF	Integrated Disposal Facility
LAW	Low Activity Waste
MTT	Main Treatment Train
NIST	National Institute of Standards and Technology
NQA	Nuclear Quality Assurance
QA	Quality Assurance
QAPP	Quality Assurance Project Plan
QARD	Quality Assurance Requirements and Description
RO	Reverse Osmosis
SBS	Submerged Bed Scrubber
UV	Ultra-Violet
UV/OX	Ultra-Violet/Oxidation
VSL	Vitreous State Laboratory
WESP	Wet Electrostatic Precipitator
WTP	Hanford Tank Waste Treatment and Immobilization Plant
WRPS	Washington River Protection *Solutions*, LLC

SECTION 1.0
INTRODUCTION

1.1 Background

The Hanford Site Effluent Treatment Facility (ETF) currently treats aqueous waste streams that include condensates from the 242-A evaporator, leachate from the Environmental Restoration Disposal Facility (ERDF), as well as laboratory wastes and, in the future, will treat liquid effluents from the Hanford Tank Waste Treatment and Immobilization Plant (WTP) and Integrated Disposal Facility (IDF) leachate. Liquid effluents from the WTP will have significant concentrations of acetonitrile. Acetonitrile is formed by reaction of nitrates and sugar in the WTP low activity waste (LAW) melters and is prevalent in the submerged bed scrubber (SBS) and wet electrostatic precipitator (WESP) liquid effluents from WTP off-gas treatment [1, 2]. When these liquids are concentrated in the WTP Effluent Management Facility (EMF) evaporator in the direct feed low activity waste (DFLAW) flow-sheet, testing has shown that the majority of the acetonitrile partitions to the evaporator condensate [3, 4]. Since the evaporator condensate is directed to the ETF, this creates a potential issue with the ETF waste acceptance criteria. Consequently, there is a need to validate flow-sheet assumptions on the fate of acetonitrile and other organics within the ETF. The present plan includes the addition of a steam stripper to the ETF to remove acetonitrile. There is, therefore, also a need to determine a suitable method to destroy acetonitrile in the overhead condensate stream from the new steam stripper.

Washington River Protection *Solutions*, LLC (WRPS) previously contracted with Atkins and the Vitreous State Laboratory (VSL) of The Catholic University of America (CUA) to perform development and testing work to evaluate potential methods for destruction of acetonitrile in WTP secondary liquid effluents. Based on the results of that work [5-7], WRPS requested that follow-on testing be conducted to further evaluate acetonitrile destruction in the steam stripper condensate using ultraviolet oxidation (UV/OX) with persulfate [8]. WRPS also requested testing to assess the rejection rate[1] of organics in the reverse osmosis (RO) system installed in the ETF [8]. This report presents the results from testing to address those needs.

1.2 Test Objectives and Scope of Work

This work was conducted according to a Test Plan [9] that is responsive to the WRPS statement of work [8].

[1] rejection rate = (1-Cp,i/Cf,i)*100, where Cp,i is the concentration of species i in the permeate and Cf,i is the concentration of species i in the feed.

In FY19 VSL completed tests with a variety of UV activated oxidants and found that the persulfate ion ($S_2O_8^{-2}$) provided rapid and complete destruction of acetonitrile under certain conditions [5, 6]. In contrast, the oxidant currently employed at ETF, hydrogen peroxide, had little effect on acetonitrile concentrations. Persulfate was also able to oxidize the other organic compounds that are predicted to be present within the ETF feed. FY20 work included testing on a new larger (~14 L) reactor system that was designed to represent a full-scale transverse section through one of the new Calgon UV/OX reactor tubes to be installed in the ETF [7]. This test system was designed such that the UV lamp power could be varied and could achieve the same UV intensity as the full-scale system. One aspect of those tests assessed acetonitrile destruction rates with UV and persulfate in a simulant for the steam stripper overhead condensate. Those tests covered a wide range of possible operating conditions and have defined a region where a treatment system could destroy acetonitrile at rates equal to the mass flow rate in the steam stripper condensate stream. One of the objectives of the FY21 work is to verify destruction rates at these specific operating conditions and to collect the data necessary to elucidate the degradation kinetics for acetonitrile, as well as acetamide and acetate, which were thought to be likely degradation products, at the conditions determined as favorable for treatment of the overhead condensate stream. In addition, since the acetonitrile mass flow rate in the steam stripper condensate stream is dictated by its rejection rate in the ETF RO units, testing on this unit operation was also required. Accordingly, a further objective of the present work was to design and construct a test system for the ETF RO units and perform testing to determine the rejection rates for acetonitrile and other organics.

1.3 Summary of Methods Previously Selected for Evaluation

Acetonitrile is very stable and, compared to other organics, is relatively difficult to destroy. Some of the most promising methods for destruction of acetonitrile involve photolysis using ultra-violet (UV) light [10-19]. Many such UV processes combine the use of UV light and chemical oxidants such as hydrogen peroxide to destroy organic contaminants. The UV light interacts with the hydrogen peroxide to generate hydroxyl radicals ($OH^{\bullet}$), which are highly reactive. The hydroxyl radicals then attack the organic molecules resulting in their destruction. The reaction can be assisted by the direct photolysis of the organic molecule by the UV light, which can break or activate certain bonds making the molecule more susceptible to oxidation. Other processes include UV light alone, UV light with ozone, UV light with ferric ion, UV light with Fenton's reagent (H_2O_2/Fe^{2+}), UV light with persulfate, UV light with chlorine, UV light with ferrioxalate, and UV light with TiO_2 and with other photocatalysts [10, 12, 13]. While most of these are based on generation of hydroxyl radicals, others generate sulfate or chlorine ($SO_4^{-\bullet}$ or $^{\bullet}Cl$) radicals [14, 16, 18, 19].

In the previous work [6], several such combinations of UV light and chemical additives were tested, including:

- UV light + hydrogen peroxide
- UV light + Fenton's reagent

- UV light + ferrioxalate
- UV light + persulfate
- UV light + hypochlorite.

Based on the results of that work [6] and subsequent testing [7], UV light + persulfate was selected for the testing with the stream stripper waste simulant in the present work.

1.4 Quality Assurance

This work was performed under a quality assurance (QA) program compliant with the applicable criteria of 10 CFR 830.120; the American Society of Mechanical Engineers (ASME) Nuclear Quality Assurance (NQA)-1, 2008 including NQA-1a 2009 Addenda, and Department of Energy (DOE) Order 414.1D, Quality Assurance. These QA requirements are implemented through a Quality Assurance Project Plan (QAPP) for WRPS work [20] that is conducted at the VSL. Test and procedure requirements by which the testing activities are planned and controlled are also defined in this plan. The program is supported by VSL standard operating procedures that were used for this work [21]. This is LAW work and is therefore not subject to the requirements of DOE/RW-0333P, Office of Civilian Waste Management Quality Assurance Requirements and Description (QARD).

SECTION 2.0
UV/OX TEST SYSTEM

2.1 Large-Scale Reactor Test Setup

Each of the three planned Calgon reactor units for the ETF consists of eight reaction tubes in series. Each of the eight tubes are approximately 1.1 m long with a central UV lamp along its length, forming a toroidal cavity through which the process fluid flows. As described previously [7], the basis of design for the new large-scale test reactor, used in previous testing [7] and for the present work, was a full-scale transverse cross-section through one of the full-scale reactors but smaller in length (0.17 m). Since the test system is designed as a batch reactor, other design features included stirring to simulate fluid flow, active temperature control to manage the heat from the lamp, and variable lamp power up to the same UV intensity as the full-scale system. To span the required range of UV power, the system was designed to accept two sizes of UV lamps (450 W and 4800 W); all of the tests in the present work used the 4800 W lamp. A cross-sectional diagram of the test system is shown in Figure 2.1; a photograph of the system is shown in Figure 2.2.

The large-scale reactor has a total volume of 14.68 L; all tests were conducted with a fluid volume of 14.0 L. The vendor specifications for the 4800-W Hanovia medium pressure mercury lamp are listed in Table 2.1. The reactor is a cylindrical jacketed stainless reaction vessel with the lamp cavity located along its axis. The lamp cavity is formed from two concentric quartz tubes which have fittings to allow cooling water to flow between them. Other fittings allow nitrogen to be flowed through the inner tube, which contains the lamp, which prevents ozone generation and provides some cooling. The reactor is fitted with a mechanical stirrer and a variety of ports for liquid introduction and sampling. The fluid cavity is sealed. The reactor is equipped with pH, temperature, and pressure sensors for monitoring these parameters throughout testing. These data were recorded using a custom LabVIEW control and data acquisition system. The temperature of the reactor contents is maintained by circulating water through both the exterior reactor jacket and between walls of the quartz cavity surrounding the UV lamp. This type of arrangement is necessary due to the very high operating temperature of the medium pressure mercury lamp, which reaches a surface temperature of ~900°C.

For each test, the waste simulant solution was first pumped by means of a peristaltic pump into the reactor. The liquid in the reactor is continuously stirred during testing. The UV lamp is initially blinded with a tubular metal shutter for the duration of lamp heat-up period (~12 minutes). The initial (i.e., time zero) sample is drawn using a Luer port, the shutter is raised, and the reaction time count begins. Sampling during testing was done with a syringe connected to the aforementioned Luer port.

All tests were conducted starting with the fluid at room temperature; there was typically a gradual temperature rise (~10 ºC) over the course of the test, as described in Section 3.

2.3 Sample Analysis

The liquid samples from all of the tests were analyzed for acetonitrile using capillary gas chromatography - mass spectroscopy (GC-MS) by injection into a Purge and Trap sample concentrator.

In the Purge and Trap method, a liquid sample is first injected into a sparge vessel. During the purge stage, organics are removed from the sample by a purge gas (usually high purity helium) passing through a frit before flowing through the sample. The frit disperses the gas into finely divided bubbles allowing a large surface area of the sample to be contacted. This process allows the inert gas stream to strip the analytes from the sample matrix and concentrate them on a solid adsorbent trap. The desorb mode follows, during which the purged analytes, now trapped onto a solid sorbent, are released when the trap is heated and back-flushed with desorption gas to release and transfer the analytes of interest into the GC. The GC carrier gas is used as the desorb gas and involves switching a six-port valve to place the trap in-line with the GC column. The GC column was a 30-m Rxi-624Sil MS capillary, 0.25 mm dia., 1.40 µm film thickness.

A Tekmar Dohrmann 3100 Purge and Trap Sample Concentrator was used for liquid samples in this work together with an Agilent Technologies Model 6890 GC with 5973N Mass Selective Detector and a G1560A Split/Splitless inlet. Compounds of interest were identified using the National Institute of Standards and Technology (NIST) spectral library built into the ChemStation GC-MS analysis software and were quantified using the integrated area under the relevant peak of the chromatograph.

For measurement of acetamide, the purge and trap method is not effective. Therefore, instead, the sample was diluted 1:10 with methanol containing 87 ng/µl of 2-butanone (MEK) as an internal standard followed by 1 µl direct manual injection into the GC-MS. The GC column was a 30-m Rxi-624Sil MS capillary, 0.25 mm dia., 1.40 µm film thickness.

The sample size collected from the reactor during testing was about 5 ml. The samples were stored in a sealed amber vial until they were analyzed – usually within a few hours.

Anions, including acetate and sulfate, were measured in selected samples by ion chromatography (IC) using a Dionex DX-120 ion chromatograph. The DX-120 consists of a CDM-3 conductivity detector and an anion self-regenerating suppressor, and was equipped with IonPac AS-14/AG-14 column/column guard for anion separation. Column elution was performed with a solution of Na_2CO_3/$NaHCO_3$. The instrument was controlled using the Chromeleon (version 6.50) data system software. Calibration standards were prepared with NIST traceable standards.

SECTION 3.0
UV/OX WASTE SIMULANT AND TEST MATRIX

3.1 Steam Stripping Simulant

The "steam stripping simulant," represents the projected composition of the waste effluent from the steam stripping process for acetonitrile removal that is being developed by WRPS. This simulant was simply a solution of acetonitrile in water to which various concentrations of persulfate oxidant (as sodium persulfate, $Na_2S_2O_8$) was added. For tests to investigate the destruction of potential reaction intermediates, acetonitrile was replaced by either acetamide or acetate, as described in the test matrix discussed below.

3.2 Test Matrix

The test matrix for this work included a combination of tests on the large reactor with the steam stripping simulant with either acetonitrile, acetamide, or acetate. The test matrix for this work is shown in Table 3.1.

All of the tests were started with a fully warm UV lamp so that the solution was exposed to a constant light intensity for the duration of the tests. As described in Section 2, this was accomplished with the shutter arrangement in the test system and the exposure time began when the shutter was opened. Sampling was conducted at a sufficient frequency to adequately define the time dependent destruction of the organics. Based on the results from FY20 testing [7], sampling times of 0, 1, 2, 3, 5, 10, 15, and 30 minutes were used. The samples were analyzed for acetonitrile, acetamide, acetate, and sulfate, as described in Section 2. All tests started with the fluid at room temperature. The temperature and pH were measured continuously during the tests.

SECTION 4.0
UV/OX RESULTS AND DISCUSSION

4.1 Acetonitrile Destruction

Table 4.1 shows the results from tests investigating the destruction of acetonitrile, without persulfate and at two different ratios of persulfate to acetonitrile. Note that there was an analytical instrument (GC-MS) issue that affected the results for acetonitrile for samples from tests LR-T2 and LR-T3, so these were repeated as Tests LR-3R and LR3A; therefore, the results for acetonitrile from the repeat tests are preferred. The results for other analytes were not affected by this issue. Up to the first five minutes, the results show more extensive destruction of acetonitrile for the tests with the lower concentration of persulfate. However, after that time, the reverse is true and at 30 minutes, the higher concentration tests yield over 90% destruction as compared to about 70% for the lower concentration tests.

4.2 Acetamide Destruction

Table 4.2 shows the results from tests investigating the destruction of acetamide at two different ratios of persulfate to acetamide. The results show that persulfate is also very effective in destroying acetamide but the variation with persulfate concentration is different from that observed for acetonitrile, with the higher concentration of persulfate yielding greater destruction at all times. At 30 minutes, the higher concentration tests yield over 99% destruction as compared to about 70 - 80% for the lower concentration tests.

4.3 Acetate Destruction

Table 4.3 shows the results from tests investigating the destruction of acetate, at two different ratios of persulfate to acetate. The results show that persulfate is also very effective in destroying acetate. The variation with persulfate concentration is more similar to that observed for acetamide than that for acetonitrile, with the higher concentration of persulfate yielding greater destruction at all times except at 15 and 30 minutes. At 15 and 30 minutes, the lower concentration tests gave slightly greater destruction than the higher concentration tests but all of them are over 95% destruction. As was the case for acetamide, the tests with the higher persulfate concentration gave over 90% acetate destruction by about ten minutes, whereas that was reached only at 30 minutes for acetonitrile, reflecting the greater difficulty of destruction of acetonitrile. At the lower persulfate concentration, acetate destruction exceeded 90% (over 95%) by about 15 minutes, whereas that was not achieved even at 30 minutes for acetonitrile or acetamide.

4.4 Acetamide Formation

Table 4.4 shows the results for the formation of acetamide in tests with acetonitrile and persulfate at two different ratios of persulfate to acetonitrile. The results show that the acetamide concentrations are below the detection limit for both tests and all test times, corresponding to less than 0.1% conversion of acetonitrile to acetamide. In view of the relative rates of destruction of acetonitrile and acetamide discussed in Sections 4.1 and 4.2, respectively, it seems unlikely that acetamide is being formed from the destruction of acetonitrile and then itself being destroyed rapidly enough to maintain concentrations below the detection limit. Therefore, the results indicate that acetamide is not a significant degradation product of the photolytic reaction of acetonitrile with persulfate.

4.5 Acetate Formation

Table 4.5 shows the results for the formation of acetate in tests with acetonitrile and persulfate at two different ratios of persulfate to acetonitrile. In both cases, the results show that the formation of acetate increases monotonically with time reaching about 20% by 30 minutes. In view of the more rapid rate of destruction of acetate than acetonitrile discussed in Section 4.3, a substantial buildup of acetate would not be expected even if the degradation of acetonitrile proceeds quantitatively via acetate. Therefore, the results are consistent with acetate being a significant degradation product of the photolytic reaction of acetonitrile with persulfate.

4.6 Sulfate Formation

Table 4.6 shows the results for the formation of sulfate in tests with acetonitrile and persulfate at two different ratios of persulfate to acetonitrile and in tests with acetate and persulfate at two different ratios of persulfate to acetate. The conversion of persulfate to sulfate is rapid, reaching about 60% in the first three minutes at the lower persulfate concentration and over 40% at the higher persulfate concentration. In all cases, up to the first ten minutes the sulfate formation percentage is lower for the tests with the higher persulfate concentration than for the corresponding tests with the lower persulfate concentration. Beyond that point, the conversion of persulfate to sulfate is essentially complete in all cases.

4.7 pH and Temperature

The large reactor is equipped with pH and temperature sensors for monitoring these parameters throughout testing. These data were recorded using a custom LabVIEW control and data acquisition system and are shown in Figures 4.1 and 4.2. All tests were conducted starting with the fluid at room temperature (~26 ^{o}C) and there was a rapid initial rise in temperature which slowed over the course of the test with the temperature stabilizing at about 37 ^{o}C.

Table 4.7 lists the initial and final pH and temperature for each test. In all tests except for LR-T1, which did not include persulfate, the pH decreased from its initial value and stabilized between about 1.6 - 2.

SECTION 5.0
UV/OX PROCESS MODELING

This section describes an analysis of the observed acetonitrile destruction data in terms of simple kinetic models to determine rate constants that together allow for extrapolation of the results to project the performance of the full-scale ultra-violet/oxidation (UV/OX) system at ETF. The approach follows closely that reported previously [6, 7].

A variety of models for UV/OX processes in general, and persulfate processes in particular, have been reported, many of which employ reaction networks involving dozens of reactions [11, 13, 15, 16, 22, 23, 24]. The model developed previously [6, 7] included kinetic equations for several chemical reactions as well as:

- Effect of UV intensity at wavelengths other than 254 nm;
- Effects of non-planar geometry;
- Effects of reflections from stainless steel reactor surfaces.

The key elements of the model are summarized below.

5.1 UV Power Absorbed

The model considers a UV/OX reactor composed of coaxial cylinders of length L. The inner cylinder of radius r_1 is the UV source and the outer cylinder of radius r_2 is the body of the reaction cell; the annulus between the cylinders contains the fluid that is being treated. If we define I_0 as the incident intensity (at r_1), then the energy absorbed per unit time (power) per unit volume of liquid is [6]:

$$P_v = \frac{2r_1}{r_2^2 - r_1^2} I_0 (1 - \mu e^{-2c\varepsilon'(r_2 - r_1)} - (1 - \mu) e^{-c\varepsilon'(r_2 - r_1)}), \qquad (5.1)$$

where c is the concentration of the absorbing species (persulfate in the present work) in the solution, μ is the reflectance of the surface at r_2, and ε' is the Naperian extinction coefficient of the absorbing species. The reflectance of UV at about 254 nm from stainless steel is about 40% [27]. The relationship between Naperian and decadic extinction coefficients, ε, is:

$$\varepsilon' = \varepsilon \ln 10;$$

typically, decadic extinction coefficients are the values quoted in the literature.

5.2 Kinetic Model for Persulfate

5.2.1 Basic Model

The kinetic model for persulfate developed previously [6, 7] is summarized in this section. We consider a simple model that employs just two reactions: the photolysis of persulfate to produce sulfate radical ions and the subsequent reaction of those radical ions with acetonitrile:

$$S_2O_8^{2-} + h\nu \rightarrow 2SO_4^{-\bullet} \tag{5.2}$$

$$SO_4^{-\bullet} + CH_3CN \rightarrow decomposition\ products\,. \tag{5.3}$$

The rate equation for the persulfate concentration as a result of its consumption via Eq. 5.2 is:

$$\frac{d[S_2O_8^{2-}]}{dt} = -(\Phi K P_v)_{254} - (\Phi K P_v)_{185}, \tag{5.4}$$

where Φ is the quantum yield for Eq. 5.2 and K is the number of moles of photons of frequency ν per joule; the first term on the right is for absorption at 254 nm and the second is for absorption at 185 nm. Note that P_v, which is given by Eq. 5.1, depends on the concentration of the absorbing species (persulfate) through $c = [S_2O_8^{2-}]$.

The rate equation for the acetonitrile concentration as a result of its consumption via Eq. 5.3 is:

$$\frac{d[CH_3CN]}{dt} = -k_1[SO_4^{-\bullet}][CH_3CN]\,, \tag{5.5}$$

where k_1 is the rate constant for Eq. 5.3.

Finally, the rate equation for the sulfate radical ion concentration as a result of its generation via Eq. 5.2 and consumption via Eq. 5.3 is:

$$\frac{d[SO_4^{-\bullet}]}{dt} = (2\Phi K P_v)_{254} + (2\Phi K P_v)_{185} - k_1[SO_4^{-\bullet}][CH_3CN]. \tag{5.6}$$

In the present work, based on the lamp characteristics listed in Table 2.1, only a single UV line (at 254 nm) was used, and all of the UV power was allocated to that line. Thus, Eq. 5.4 becomes:

$$\frac{d[S_2O_8^{2-}]}{dt} = -(\Phi K P_v)_{254}, \tag{5.7}$$

and Eq. 5.6 becomes:

$$\frac{d[SO_4^{-\bullet}]}{dt} = (2\Phi K P_v)_{254} - k_1[SO_4^{-\bullet}][CH_3CN]. \tag{5.8}$$

With the initial concentrations of persulfate and acetonitrile together with the parameter values defined by the experimental conditions and values from the literature (see below), the only unknown is the rate constant k_1. Thus, this system of differential equations can be solved numerically and the value of k_1 determined by least squares regression to best fit the available data.

It is noted that simplified models, such as those employed here, that do not include terminating reactions that quench each and every radical will predict that those radicals are still present at the end of the reaction, which is, of course, not realistic. Since it is well known that radical lifetimes are typically very short and that there are many diverse quenching mechanisms, even much more complex reaction networks often do not bother to address this issue. Furthermore, there are typically large number of radicals in play (for persulfate, for example, this includes $SO_4^{-\cdot}$, $HO^{\cdot}$, $S_2O_8^{-\cdot}$, $Cl^{\cdot}$, $Cl_2^{-\cdot}$, $ClO_2^{\cdot}$, $ClHO^{-\cdot}$, $CO_3^{-\cdot}$, etc.).

5.2.2 Extended Model

In previous work [7] an extended model was developed to address some of the observed deficiencies in the model described in Section 5.2.1. The extended model includes an additional process that consumes sulfate radical ions. One of the most significant such reactions is the reaction with water according to [11, 15]:

$$SO_4^{-\bullet} + H_2O \rightarrow HO^{\bullet} + HSO_4^{-} \tag{5.9}$$

$$HO^{\bullet} + S_2O_8^{2-} \rightarrow HSO_4^{-} + SO_4^{-\bullet} + \tfrac{1}{2}O_2. \tag{5.10}$$

These reactions consume and regenerate a sulfate radical ion but the net result is the destruction of one persulfate ion. The rate equation for the hydroxyl radical concentration is then:

$$\frac{d[HO^{\bullet}]}{dt} = k_3[H_2O][SO_4^{-\bullet}] - k_4[HO^{\bullet}][S_2O_8^{2-}]. \tag{5.11}$$

If we assume a steady state for $[HO^{\bullet}]$, then $d[HO^{\bullet}]/dt = 0$ and therefore:

$$k_3[H_2O][SO_4^{-\bullet}] = k_4[HO^\bullet][S_2O_8^{2-}]. \quad (5.12)$$

We next add this new consumption mechanism into the rate equation for $[S_2O_8^{2-}]$ (Eq. 5.7) to give:

$$\frac{d[S_2O_8^{2-}]}{dt} = -(\Phi K P_v)_{254} - k_4[HO^\bullet][S_2O_8^{2-}]; \quad (5.13)$$

Substituting Eq. 5.12, we obtain:

$$\frac{d[S_2O_8^{2-}]}{dt} = -(\Phi K P_v)_{254} - k_3[H_2O][SO_4^{-\bullet}]. \quad (5.14)$$

The net result is that in the extended model, Eq. 5.7 is replaced by Eq. 5.14 and one additional parameter (k_3) is added; however, it is convenient to take that parameter to be $k_3[H_2O]$ since $[H_2O]$ is essentially constant at about 55.6 mol/L. The data sets for tests from the present work investigating acetonitrile destruction with persulfate, together with data from previous tests with the steam stripping simulant [7], were analyzed with this model, as described below. The analysis included provisions to prevent the concentrations from going negative, which is otherwise possible via Eq. 5.14.

5.3 Data Sets and Parameter Values

5.3.1 Overview

Data from tests with the steam stripping simulant examining acetonitrile destruction were used for modeling. There are four such tests from the present work plus four such tests on the large reactor from previous work [7]. However, the four tests in the present work relate to two pairs of duplicate tests and therefore only two different conditions. The tests and test conditions are listed in Table 5.1.

The values of the parameters in the model are listed in Tables 5.2. The intensities were calculated from the respective UV lamp specifications, as described in Section 5.4.2. Literature data were used for the quantum yield [11, 15, 25 - 30] and extinction coefficients of persulfate [11, 15, 25 - 30], and for the reflectance of stainless steel [31].

5.3.2 Calculation of Lamp Intensities

The lamp intensities were calculated in the same manner as described previously [6, 7].

All of the tests in the present work used a 4800 W lamp with specifications listed in Table 2.1. Some of the tests in previous work [7] also used a 450 W lamp. For each lamp, the

UV power for all UV-B and UV-C lines was summed and assigned to the 254 nm line for the purpose of modeling. This information was used to calculate the intensities at r_1, which is I_0. It is noted, however, that, in principle, the two terms for the UV lines at 254 nm and 185 nm in Eq. 5.4 (and, correspondingly, with the minus signs replaced by 2 in Eq. 5.6) could be replaced by a sum over corresponding terms for each of the N UV lines listed in Table 2.1:

$$\sum_{i}^{N} -(\Phi K P_v)_i \, . \tag{5.15}$$

However, this requires knowledge of the quantum efficiency Φ and the extinction coefficient ε at every wavelength, which is not available; data for the quantum efficiency at wavelengths other than 254 nm are particularly sparse.

Many vendor specification sheets state that the intensity scales as the inverse square of the distance. However, while that is true for a point source, these lamps are essentially line sources. To address this, as in the previous work [7], a Gaussian-surface approach was employed whereby the total power emitted by the source (at a given wavelength) is equal to the integral of the intensity over a surface that completely encloses the source. This calculation is simplified if the enclosing surface is chosen to be at a constant distance from the source. Thus, if the source has a length L and radius r_1 and we enclose it with surface in the form of a coaxial cylinder of radius R with hemispherical end caps also of radius R (so that essentially all of the surface is the same distance from the source), and if the UV power emitted by the source is P, then the intensity at R is approximately:

$$I(R) = \frac{P}{(2\pi RL + \alpha 4\pi R^2)}, \tag{5.16}$$

where α is a "view factor" for the hemispherical end caps, which is expected to be less than one. Clearly, the intensity scales as $1/R^2$ only when $L/R << 1$. Conversely, if $L >> R$, then the intensity scales more like $1/R$. The view factor was estimated in the previous work [7] to be $\alpha = 0.72$.

Finally, if we set $R = r_1$, with L = 140 mm (450 W lamp) or L = 164 mm (4800 W lamp), then this gives the incident intensity (I_0) that we need. The values obtained from this calculation are provided in Table 5.1.

5.4 Modeling Results and Discussion

The extended model for persulfate described above was implemented in Mathematica (Wolfram), which was used to solve the system of differential equations and find the optimum value of the rate constants k_1 and and $k_3[H_2O]$ by minimizing the χ^2 statistic. The calculation of χ^2 employed an experimental uncertainty in the measurement of the acetonitrile concentration of 10% plus 5.76 x 10^{-6} mol/L.

Table 5.3 lists the fitted values of the rate constants k_1 and $k_3[H_2O]$ for each of the eight data sets. Each data set was fitted individually ('individual fit") and then all eight data sets were fitted simultaneously with a single pair of k_1 and $k_3[H_2O]$ values ("global fit"). Figures 5.1 – 5.8 show the acetonitrile destruction percentage for each of the eight data sets in comparison to the model results for the individual fits. Figures 5.9 – 5.16 show the corresponding predicted concentrations of all species for each of the eight data sets. Overall, the model fits provide good representations of the acetonitrile destruction data. In some cases, discontinuities in the slope of the acetonitrile destruction versus time are evident. Figures 5.9 – 5.16 show that these are due to exhaustion of the persulfate at that point, which occurs for all tests except test LR-S1. The predicted exhaustion of persulfate in Tests LR-T3A and LR-T3R (which are replicates with LR-T2), shown in Figures 5.13 and 5.14, respectively, can be compared to the measured sulfate formation percentage for Test LR-T2 in Table 4.6, which shows that the predicted exhaustion occurs somewhat earlier than measured. Figures 5.13 and 5.14 are replotted with the measured sulfate data in Figures 5.17 and 5.18, respectively, to support this comparison. Similarly, the corresponding predicted and measured exhaustion points also can be compared for Test LR-9 in Figures 5.16 and Table 4.6, respectively, which again shows that the predicted exhaustion occurs somewhat earlier than measured. Figure 5.16 is replotted with the measured sulfate data in Figures 5.19 to support this comparison.

The values of k_1 and $k_3[H_2O]$ for the global fit (0.3855 and 0.04166, respectively) are comparable to the values obtained from a global fit to data obtained in previous work [7] with a more complex ETF waste simulant (0.9235 and 0.0195, respectively), as also are the values for the individual fits to the five data sets from the present work, which span a narrower composition range than the corresponding data for the steam stripping simulant from the previous work [7].

Although the model fits the acetonitrile destruction data quite well, there is considerable variation in the values of the fitted parameters. As noted previously [7], the fact that k_1 and $k_3[H_2O]$ are not constant indicates that deficiencies still remain in the model. In particular, when other test variables are fixed, it is evident that the parameters vary with power, acetonitrile concentration at fixed ratio of persulfate to acetonitrile, and with the ratio of persulfate to acetonitrile at fixed acetonitrile concentration. From a practical perspective, the variation with power is particularly important for predicting the performance of a full-scale system but is evidently not fully captured by the present model. The limitations of the present model in that regard highlight the importance of testing at full scale conditions. In view of these issues, it is recommended that any process modeling calculations should use the model parameter values corresponding to the conditions (power, concentrations, etc.) that are closest to those of interest.

SECTION 6.0
REVERSE OSMOSIS TESTING

The primary objective of the reverse osmosis system testing in the present work was to assess the rejection rate of organics that are projected to be present in the main treatment train (MTT) feed to the ETF RO system. To accomplish this, a small-scale reverse osmosis test system was designed and installed at VSL to mimic as closely as possible the operating conditions of the ETF RO system.

6.1 System Description

The ETF RO system consists of two Stages (1 and 2) each composed of two Arrays (1 and 2) of RO elements. The two arrays in Stage 1 and the first array in Stage 2 each consist of six RO elements, while the second array in Stage 2 consists of three RO elements. Stage 1 is supplied from the First RO Feed Tank through a feed pump and discharges into the Second RO Feed Tank, which supplies Stage 2 through a feed pump. There is a booster pump between the first and second arrays in Stage 1. The RO elements are connected in parallel while the arrays are connected in series.

The RO elements split the feed liquid into two streams: the permeate, which is the liquid that has passed through the RO membrane, and the concentrate, which is the liquid that has not; the concentrate is also referred to as the reject stream.

In Stage 1, the concentrate from the first array is fed into the second array while the permeates from both arrays are collected in the Second RO Feed Tank; the concentrate from the second array is directed to the Secondary Waste Receiving Tanks. Stage 2 functions similarly except that the permeates from both arrays are directed to the polishing processes in the ETF while the concentrate is recycled back to the Stage 1 feed tank.

The RO test system for the present work was designed as a single stage with two arrays, each with a single RO element. Since the concentration of organics is highest in Stage 1, the test system was configured to represent Stage 1 of the ETF RO system; however, the system was designed such that it can be easily reconfigured to represent Stage 2. A schematic diagram of the test system is shown in Figure 6.1. A photograph of the test system is shown in Figure 6.2, In the test system, the final permeate and concentrate streams are combined and recycled to the feed tank to allow longer duration runs to be performed without requiring very large volumes of waste simulant. A 20-gallon feed tank was utilized in this testing.

The test system used the same RO elements as the ETF RO system with the full-scale length but a smaller diameter. The ETF RO system uses DuPont FilmTec BW30-8040 elements, which are brackish water elements that are 8 inches in diameter and 40 inches long. The test

system uses DuPont FilmTec BW30-2540 elements, which are 2.5 inches in diameter and 40 inches long. A photograph of a new element is shown in Figure 6.3. All of these elements use the FilmTec FT30 membrane. The FilmTec membrane is a thin-film composite membrane consisting of three layers: a polyester support web, a micro- porous polysulfone interlayer, and an ultra-thin polyamide barrier layer on the top surface; the FT30 membrane uses an aromatic polyamide [32]. The polyester web provides the primary structural support, but it is too irregular and porous to provide a proper substrate for the salt barrier layer, which is about 200 nm thick. Therefore, a micro-porous layer of polysulfone, which has surface pores controlled to a diameter of approximately 15 nm, is cast onto the surface of the web to provide the substrate for the barrier layer [32]. These membranes are packed in a spiral-wound configuration to produce an RO element [32].

Table 6.1 lists the operating parameters for the ETF RO system [8]; those parameters were matched to the extent possible in the test system. Table 6.2 compares the characteristics of the RO elements used in the ETF system and in the test system that was installed for the present work.

Figure 6.1 shows the monitoring points for flow, pressure, and the sampling points in the test system. The feed flow rate was adjusted to achieve the same flow rate per unit membrane surface area as in the ETF RO system. The tests were run for sufficiently long durations to achieve steady state conditions. Samples were analyzed for all of the organics in the feed (see Section 6.3) to determine their rejection rates for each of the two elements (representing Array 1 and Array 2). In addition, selected samples were analyzed for inorganic species to document performance in terms of salt rejection.

6.2 Waste Simulant

The reverse osmosis system testing used the waste simulant composition shown in Table 6.3. The simulant is based on the results from recent flowsheet model runs [33] and specifically gPROMS Run 3 in that document. The simulant was charge balanced and adjusted to a pH of 5.0 +/- 0.2 with sulfuric acid.

Organics were added to the simulant described above at the concentrations listed in Table 6.4. The concentrations of acetone and formate were increased from the gPROMS values per WRPS direction.

6.3 Sample Analysis

Samples collected from the RO test system were analyzed for organics by GC-MS, as described in Section 2.3. Analysis of n-Nitrosodimethylamine (NDMA) by GC-MS proved to be particularly challenging and, because of its high solubility in water, it is not amenable to purge and trap techniques. The samples were therefore extracted into methylene chloride and a 2 µL split-less pulsed injection was used with a 30-m Rtx-1701 capillary column, 0.25 mm dia., with

0.25 µm film thickness. All samples were spiked with an internal standard prior to extraction to account for extraction efficiency; isotopically labelled NDMA ($^{13}C_2D_6$, 82.1 amu versus 74.1 amu) was used for that purpose. In addition, anions were analyzed by ion chromatography and cations were analyzed by inductively coupled plasma – atomic emission spectroscopy (ICP-AES).

6.4 Test Results

The RO membrane system was operated 8 hours per day for 5 days, giving 40 hours of total run time. During testing, the pressure at the inlet and outlet of each membrane, the permeate flow from each membrane, and the concentrate flow from the second membrane were electronically recorded every 10 seconds for the duration of testing. The average, maximum, and minimum values for these parameters on each day are given in Table 6.5.

The average inlet pressure over the 5 days of testing for both membranes was between 128.9 - 133.0 psig, which is in good agreement with the target inlet pressure for the RO membranes of 130 psig. The average pressure drop was between 10.7 - 11.3 psi. The average flow rate from the feed tank (Membrane 1 Feed Flow) was between 13.4 - 13.6 lpm for all tests. The recovery, defined here as the permeate flow divided by the feed flow expressed in percent, was similar for both membranes. For Membrane 1, the recovery was between 7.9 - 8.3% and for Membrane 2, it was between 7.6 - 8.0%. The combined recovery for the two membranes was between 14.9 - 15.7%. Figures 6.4 and 6.5, respectively, show the pressure and flow measurements taken during the 40 hours of run time.

Liquid samples (~20 ml) from the feed tank as well as the concentrate and permeate from both membranes were taken at the end of each day. Additionally, on the first day of testing, a set of samples was taken ~45 minutes after starting the system. The sampling times are indicated on Figures 6.4 and 6.5.

The analysis results for acetonitrile, acetone, acrylonitrile, and NDMA are shown in Table 6.5. The results are quite stable over time and no clear trends with time are evident. Therefore, the sample data were averaged over all times and the results are summarized in Table 6.6. For each organic, the rejection rates for Membrane 1 and 2 are very similar. The highest ratios are for acetone and NDMA, which are both about 60%, followed by acrylonitrile at about 20% and acetonitrile at about 10%.

Analysis for acetate and formate by ion chromatography was complicated by their low concentrations in the feed (both 1.66 mg/L), the resulting near detection limit values in the permeate, and considerable overlap of the peaks in the chromatograms under the measurement conditions used. However, by employing a combination of mixed acetate + formate standards, it was possible to quantify the sum of acetate + formate, even though they could not be resolved at these low concentrations. The results for the permeate samples are shown in Table 6.7. These values can be used with the nominal concentrations of formate and acetate in the feed to calculate the rejection rate, which is also shown in Table 6.7. The results are very consistent

between the two membranes and at all times and show very little variation. The mean of the rejection rate values over all of the data is 90.9%.

Table 6.8 shows the results for sodium. Again, the results are very similar for the two membranes and very stable over time. The rejection rates are all above 98% except for the sample taken at the earliest time (45 minutes, 97%).

SECTION 7.0
SUMMARY AND CONCLUSIONS

One of the objectives of the present work was to further investigate a UV-persulfate process for destruction of acetonitrile in the condensate stream from a steam stripper unit that is planned for installation at the ETF. Previous testing [6, 7] covered a wide range of possible operating conditions and have defined a region where a treatment system could destroy acetonitrile at rates equal to the mass flow rate in the steam stripper condensate stream. In the present work, tests were conducted to verify destruction rates at these specific operating conditions and to collect the data necessary to elucidate the degradation kinetics for acetonitrile, as well as acetamide and acetate, which were thought to be likely degradation products, at the conditions determined as favorable for treatment of the overhead condensate stream. In addition, since the acetonitrile mass flow rate in the steam stripper condensate stream is dictated by its rejection rate in the ETF RO units, testing on this unit operation was also required. Accordingly, a further objective of the present work was to design and construct a test system for the ETF RO units and perform testing to determine the rejection rates for acetonitrile and other organics.

The UV/OX tests were conducted in the same large-scale reactor developed previously [7], which is a full-scale transverse cross-section through one of the full-scale Calgon reactor units planned for installation in the ETF but smaller in length. All of the tests in the present work employed a 4800 W lamp such that the power per unit length of reactor was the same as that in the full scale system.

To support testing to assess the rejection rate of organics that are projected to be present in the main treatment train feed to the ETF RO system, a small-scale RO test system was designed and installed at VSL to mimic the operating conditions of the ETF RO system. The test system was designed as a single stage with two arrays, each with a single RO element. The test system used the same RO elements as the ETF RO system with the full-scale length but a smaller diameter.

The principal findings from these tests are summarized below.

6.1 UV/OX Testing

- Acetonitrile Destruction: Tests at two different ratios of persulfate to acetonitrile showed that up to the first five minutes, there was more extensive destruction of acetonitrile for the tests with the lower concentration of persulfate. However, after that time, the reverse was true and at 30 minutes, the higher concentration tests yield over 90% destruction as compared to about 70% for the lower concentration tests.

- Acetamide Destruction: Tests at two different ratios of persulfate to acetamide showed that persulfate is also very effective in destroying acetamide. However, in this case, the higher concentration of persulfate gave greater destruction at all times. At 30 minutes, the higher concentration tests gave over 99% destruction as compared to about 70 - 80% for the lower concentration tests.
- Acetate Destruction: Tests at two different ratios of persulfate to acetate showed that persulfate is also very effective in destroying acetate. The variation with persulfate concentration is more similar to that observed for acetamide than that for acetonitrile, with the higher concentration of persulfate yielding greater destruction at all times except at 15 and 30 minutes, where the lower concentration tests gave slightly greater destruction, but all of them gave over 95% destruction. As was the case for acetamide, the tests with the higher persulfate concentration gave over 90% acetate destruction by about ten minutes, whereas that was reached only at 30 minutes for acetonitrile, reflecting the greater difficulty of destruction of acetonitrile. At the lower persulfate concentration, acetate destruction exceeded 90% (over 95%) by about 15 minutes, whereas that was not achieved even at 30 minutes for acetonitrile or acetamide.

In addition, the *formation* of acetamide and acetate as potential acetonitrile degradation products was monitored, as also was the formation of sulfate from the decomposition of persulfate. The following observations can be made:

- Acetamide Formation: The results for the formation of acetamide in tests with acetonitrile and persulfate at two different ratios of persulfate to acetonitrile show that the acetamide concentrations are below the detection limit for both tests and all test times, corresponding to less than 0.1% conversion of acetonitrile to acetamide. In view of the relative rates of destruction of acetonitrile and acetamide discussed above, it therefore seems unlikely that acetamide is being formed from the destruction of acetonitrile and then itself being destroyed rapidly enough to maintain concentrations below the detection limit. Therefore, the results indicate that acetamide is not a significant degradation product of the photolytic reaction of acetonitrile with persulfate.
- Acetate Formation: The results for the formation of acetate in tests with acetonitrile and persulfate at two different ratios of persulfate to acetonitrile show that, in both cases, the formation of acetate increases monotonically with time, reaching about 20% by 30 minutes. In view of the more rapid rate of destruction of acetate than acetonitrile discussed above, a substantial buildup of acetate would not be expected even if the degradation of acetonitrile proceeds quantitatively via acetate. Therefore, the results are consistent with acetate being a significant degradation product of the photolytic reaction of acetonitrile with persulfate.
- Sulfate Formation: Sulfate formation was measured in tests with acetonitrile and persulfate at two different ratios of persulfate to acetonitrile and in tests with acetate and persulfate at two different ratios of persulfate to acetate. The conversion of persulfate to sulfate is rapid, reaching about 60% in the first three minutes at the lower persulfate concentration and over 40% at the higher persulfate concentration. In all cases, up to the

first ten minutes the sulfate formation percentage is lower for the tests with the higher persulfate concentration than for the corresponding tests with the lower persulfate concentration. Beyond that point, the conversion of persulfate to sulfate is essentially complete in all cases.

Data from tests with the steam stripping simulant examining acetonitrile destruction were used for modeling. There are four such tests from the present work plus four such tests on the large reactor from previous work [7]. However, the four tests in the present work relate to two pairs of duplicate tests and therefore only two different conditions. These data were analyzed in terms of the extended kinetic model for persulfate developed previously [7]. The principal findings are summarized as follows:

- Overall, the model fits provide good representations of the acetonitrile destruction data.
- In some cases, discontinuities in the slope of the acetonitrile destruction versus time are evident in the model results, which are due to exhaustion of the persulfate at that point. However, where comparisons can be made with measured sulfate formation data, the results show that the predicted exhaustion occurs somewhat earlier than measured.
- The values of the model rate parameters, k_1 and $k_3[H_2O]$, for the global fit (0.3855 and 0.04166, respectively) are comparable to the values obtained from a global fit to data obtained in previous work [7] with a more complex ETF waste simulant (0.9235 and 0.0195, respectively), as also are the values for the individual fits to the five data sets from the present work, which span a narrower composition range than the corresponding data for the steam stripping simulant from the previous work [7].
- Although the model fits the acetonitrile destruction data quite well, there is considerable variation in the values of the fitted parameters, indicating that deficiencies still remain in the model.
- In particular, when other test variables are fixed, it is evident that the parameters vary with power, acetonitrile concentration at fixed ratio of persulfate to acetonitrile, and with the ratio of persulfate to acetonitrile at fixed acetonitrile concentration.
- From a practical perspective, the variation with power is particularly important for predicting the performance of a full-scale system but is evidently not fully captured by the present model.
- The limitations of the present model in that regard highlight the importance of testing at full scale conditions.
- In view of these issues, it is recommended that any process modeling calculations should use the model parameter values corresponding to the conditions (power, concentrations, etc.) that are closest to those of interest.

6.2 Reverse Osmosis Testing

- The RO membrane system was operated 8 hours per day for 5 days, giving 40 hours of total run time. The pressures and flows were very stable over that time.

- The recovery, defined here as the permeate flow divided by the feed flow expressed in percent, was between 7.9 - 8.3% and 7.6 - 8.0% for Membranes 1 and 2, respectively. The combined recovery for the two membranes was between 14.9 - 15.7%.

- The results for the concentrations of acetonitrile, acetone, acrylonitrile, and NDMA in the various streams were quite stable over time and no clear trends with time are evident. The results for both membranes are very similar.

- When the data are averaged over all times, the rejection rates are highest for acetone and NDMA, which are both about 60%, followed by acrylonitrile at about 20% and acetonitrile at about 10%.

- The results for the concentrations of acetate plus formate (combined) are very consistent between the two membranes and at all times and show very little variation. The mean of the rejection rate values over all of the data is 90.9%.

- The results for the concentrations of sodium are very similar for the two membranes and very stable over time. The rejection rates are all above 98% except for the sample taken at the earliest time (45 minutes, 97%).

SECTION 8.0
REFERENCES

[1] "Compilation of Off-Gas Vapor and Liquid Phase Organic Information from Scale Melter Testing of LAW Simulants," K.S. Matlack and I.L. Pegg, VSL-17S4450-1, Rev. 0, Vitreous State Laboratory, The Catholic University of America, Washington, DC, 12/13/17.

[2] "Estimates of Acetonitrile Generation from Scale Melter Testing of LAW Simulants," K.S. Matlack and I.L. Pegg, Summary Report, VSL-19S4573-1, Rev. A, Vitreous State Laboratory, The Catholic University of America, Washington, DC, 10/10/19.

[3] "DFLAW Glass and Feed Qualifications with AP-107 to Support WTP Start-Up and Flow-Sheet Development," K.S. Matlack, H. Abramowitz, I.S. Muller, I. Joseph, and I.L. Pegg, Final Report, VSL-18R4500-1, Rev. 0, Vitreous State Laboratory, The Catholic University of America, Washington, DC, 9/27/18.

[4] "EMF Evaporation Testing to Support WTP Start-Up and Flowsheet Development," K.S. Matlack, H. Abramowitz, M. Brandys, and I.L. Pegg, Final Report, VSL-19R4640-1, Rev. 0, Vitreous State Laboratory, The Catholic University of America, Washington, DC, 9/30/19.

[5] "Treatment for Acetonitrile," M. Brandys and I.L. Pegg, Summary Report, VSL-19S4730-1, Rev. 0, Vitreous State Laboratory, The Catholic University of America, Washington, DC, 10/20/19.

[6] "Testing of UV Oxidation Process for Acetonitrile Destruction," M. Brandys, N.A. Mecholsky, H. Abramowitz, R. Cecil, and I. L. Pegg, Final Report, VSL-20R4730-1, Rev. 0, Vitreous State Laboratory, The Catholic University of America, Washington, DC, 7/31/20.

[7] "Acetonitrile Destruction in ETF Feed Solutions by UV/OX and Persulfate," M. Brandys, N.A. Mecholsky, H. Abramowitz, R. Cecil, and I. L. Pegg, Final Report, VSL-20R4850-1, Rev. 0, Vitreous State Laboratory, The Catholic University of America, Washington, DC, 2/11/21.

[8] "Testing to Address the Fate Acetonitrile Destruction in the ETF," Statement of Work, Requisition # 346634, Rev. 0, Washington River Protection *Solutions*, Richland, WA, January 19, 2021.

[9] "Acetonitrile Destruction and Fate of Organics in the Reverse Osmosis System at the ETF," M. Brandys, H. Abramowitz, and I.L. Pegg, Test Plan, VSL-21T5050-1, Rev. 0, Vitreous State Laboratory, The Catholic University of America, Washington, DC, 5/4/21.

[10] "A Review on the Degradation of Organic Pollutants in Waters by UV Photoelectro-Fenton and Solar Photoelectro-Fenton," E. Brillas, J. Braz. Chem. Soc., 25, 393 (2014).

[11] "Degradation of Acetonitrile Residues Using Oxidation Processes," R.C. da C. M. Micaroni, M. Izabel, M.S. Bueno, and W. de F. Jardim, J. Braz. Chem. Soc., 15, 509 (2004).

[12] "Photocatalytic Oxidation of Acetonitrile in Gas–Solid and Liquid–Solid Regimes," M. Addamo, V. Augugliaro, S. Coluccia, M. Giulia Faga, E. Garcia-Lopez, V. Loddo, G. Marci, G. Martra, and L. Palmisano, Journal of Catalysis 235, 209 (2005).

[13] "Photocatalytic Oxidation of Acetonitrile in Aqueous Suspension of Titanium Dioxide Irradiated by Sunlight," V. Augugliaro, A. Bianco Prevot, J. Caceres Vazquez, E. Garcıa-Lopez, A. Irico, V. Loddo, S. Malato Rodrıguez, G. Marcı, L. Palmisano, and E. Pramauro, Advances in Environmental Research, 8, 329 (2004).

[14] "Sulfate Radical-Based Water Treatment in Presence of Chloride: Formation of Chlorate, Inter-Conversion of Sulfate Radicals into Hydroxyl Radicals and Influence of Bicarbonate, H. V. Lutze, N. Kerlin, T. C. Schmidt, Water Research, 72, 349 (2015).

[15] Ferrioxalate-Mediated Solar Degradation of Organic Contaminants in Water," A. Safarzadeh-Amiri, J. R. Bolton, and S. R. Cater, Solar Energy, 56, 439, (1996).

[16] Synergistic Effect Between UV and Chlorine (UV/Chlorine) on the Degradation of Carbamazepine: Influence Factors and Radical Species," W. Wang, Q. Wu, N. Huang, T. Wang, and H. Hu, Water Research, 98, 190 (2016).

[17] "Review of Photochemical Reaction Constants of Organic Micropollutants Required for UV Advanced Oxidation Processes in Water," B.A. Wols and C.H.M. Hofman-Caris, Water Research, 46, 2815 (2012).

[18] "Impact of Chloride Ions on UV/H2O2 and UV/Persulfate Advanced Oxidation Processes," W. Zhang, S. Zhou, J. Sun, X. Meng, J. Luo, D. Zhou, J. Crittenden, Environ. Sci. Technol., 52, 7380 (2018).

[19] "Oxidation Mechanisms of the UV/Free Chlorine Process: Kinetic Modeling and Quantitative Structure Activity Relationships," S. Zhou, W. Zhang, J. Sun, S. Zhu, K. Li, X. Meng, J. Luo, Z. Shi, D. Zhou, and J. C. Crittenden, Environ. Sci. Technol., 53, 4335, (2019).

[20] "Quality Assurance Project Plan for WRPS Support Activities Conducted by VSL," VSL-QAPP-WRPS, Rev. 5, Vitreous State Laboratory, The Catholic University of America, Washington, DC, 9/30/19.

[21] "Master List of Controlled VSL Manuals and Standard Operating Procedures in Use," QA-MLCP, Rev. 176, Vitreous State Laboratory, The Catholic University of America, Washington, DC, 9/24/21.

[22] "UVA-UVB Activation of Hydrogen Peroxide and Persulfate for Advanced Oxidation Processes: Efficiency, Mechanism and Effect of Various Water Constituents," W. Huang, A. Biancoa, M. Brigantea, and G. Mailhot, J. Hazardous Materials, 347, 279 (2018).

[23] "The Photolysis of Potassium Peroxodisulphate in Aqueous Solution in the Presence of tert-Butanol: a Simple Actinometer for 254 nm Radiation," G. Mark, M.N. Schuchmann, H.-P. Schuchmann, C. von Sonntag, J. Photochem. Photobiol. A: Chemistry, 55, 157 (1990).

[24] "A Mechanistic Understanding of the Degradation of Trace Organic Contaminants by UV/Hydrogen Peroxide, UV/Persulfate and UV/Free Chlorine for Water Reuse, W. Li, T. Jain, K. Ishida and H. Liu, Environ. Sci.: Water Res. Technol., 3, 128 (2017).

[25] "Probing the Radical Chemistry in UV/Persulfate-Based Saline Wastewater Treatment: Kinetics Modeling and Byproducts Identification," R. Yuan, Z. Wang, Y. Hub, B. Wanga, S. Gao, Chemosphere, 109, 106 (2014).

[26] "UVA-UVB Activation of Hydrogen Peroxide and Persulfate for Advanced Oxidation Processes: Efficiency, Mechanism and Effect of Various Water Constituents," W. Huang, A. Biancoa, M. Brigantea, and G. Mailhot, J. Hazardous Materials, 347, 279 (2018).

[27] "The Photolysis of Potassium Peroxodisulphate in Aqueous Solution in the Presence of tert-Butanol: a Simple Actinometer for 254 nm Radiation," G. Mark, M.N. Schuchmann, H.-P. Schuchmann, C. von Sonntag, J. Photochem. Photobiol. A: Chemistry, 55, 157 (1990).

[28] "A Mechanistic Understanding of the Degradation of Trace Organic Contaminants by UV/Hydrogen Peroxide, UV/Persulfate and UV/Free Chlorine for Water Reuse, W. Li, T. Jain, K. Ishida and H. Liu, Environ. Sci.: Water Res. Technol., 3, 128 (2017).

[29] "Degradation of Acetic Acid with Sulfate Radical Generated by Persulfate Ions Photolysis," J. Criquet, N. Karpel, V. Leitner, Chemosphere, 77 194 (2009).

[30] "On the Photolysis of Simple Anions and Neutral Molecules as Sources of O^-/OH, SO_x^- and Cl in Aqueous Solution," H. Herrmann, Phys. Chem. Chem. Phys., 9, 3935 (2007).

[31] "Procedures and Standards for Accurate Spectrophotometric Measurements of Specular Reflectance, J.C. Zwinkels, M. Noel, and C.X. Dodd, Applied Optics, 33, 7933 (1994).

[32] "FilmTec™ Reverse Osmosis Membranes Technical Manual," Version 7, DuPont Water Solutions, February 2021.

[33] "Dynamic ETF gPROMS Model (ETFD-SR-02) Scenario Acceptance Test Report," C.R. Kimura, RPP-RPT-62933, Revision 1, Washington River Protection Solutions, Richland, WA, April 2021.

Table 2.1. Vendor Specifications for the Hanovia Medium Pressure Mercury UV Lamp Used in the Large Reactor.

Lamp Model		**6906A453**
Lamp Power (nom.), [W]		4800
Lamp Voltage, $[V]_{rms}$		390±20
Lamp Current, $[A]_{rms}$		12.5
Mercury Line, [nm]	Band	Radiated Energy, [W]
1367.3	IR	36.9
1128.7		25.2
1014.0		115
578.0 (Y)	VIS	252
546.1 (G)		147
435.8 (B)		193
404.5 (V)		88.1
366.0	UVA	353
334.1		25.2
313.0	UVB	184
302.5		120
296.7		55.3
289.4		16.1
280.4		50.6
275.3	UVC	15.3
270.0		17.7
265.2		101
257.1		22.9
253.7		87.7
248.2		36.9
240.0		26.6
238.0		30.6
236.0		22.6
232.0		27.8
222.4		33.5
Total, [W]		2086

Table 3.1. Test Matrix for UV/OX Testing with Steam Stripper Simulant and Persulfate.

Test	Lamp Power (W)	Initial Acetonitrile (g/L)	Initial Acetamide (g/L)	Initial Acetate (g/L)	Initial Persulfate Anion (g/L)
1	4800	0.6	0	0	0.00
2	4800	0.6	0	0	4.21
3	4800	0.6	0	0	4.21
4	4800	0	0.86	0	4.21
5	4800	0	0.86	0	4.21
6	4800	0	0	0.86	4.21
7	4800	0	0	0.86	4.21
8	4800	0.6	0	0	8.42
9	4800	0.6	0	0	8.42
10	4800	0	0.86	0	8.42
11	4800	0	0.86	0	8.42
12	4800	0	0	0.86	8.42
13	4800	0	0	0.86	8.42

Table 4.1. Acetonitrile Destruction Results from Large Reactor Tests with Steam Stripping Simulant and Acetonitrile.

Test	Lamp Power, W	Acetonitrile Concentration		$S_2O_8^{2-}$ to Acetonitrile Mole Ratio	$S_2O_8^{2-}$ Concentration		Acetonitrile Destruction vs. Time (minutes)							
		g/L	mol/L		mol/L	g/L	0	1	2	3	5	10	15	30
LR-T1	4800	0.6	1.46E-02	0	0	0	0.0%	-0.1%	4.6%	5.6%	1.1%	3.4%	3.0%	6.8%
LR-T2	4800	0.6	1.46E-02	1.5	2.19E-02	4.21	0.0%	11.4%	26.8%	37.3%	50.5%	59.2%	55.4%	60.3%
LR-T3	4800	0.6	1.46E-02	1.5	2.19E-02	4.21	0.0%	22.3%	28.7%	29.4%	38.7%	34.7%	45.0%	48.7%
LR-T3R	4800	0.6	1.46E-02	1.5	2.19E-02	4.21	0.0%	26.5%	39.8%	45.8%	65.5%	67.3%	71.1%	71.6%
LR-T3A	4800	0.6	1.46E-02	1.5	2.19E-02	4.21	0.0%	23.4%	35.3%	44.3%	55.2%	65.7%	67.7%	70.8%
LR-T8	4800	0.6	1.46E-02	3	4.38E-02	8.42	0.0%	11.0%	22.5%	31.7%	48.6%	74.5%	87.6%	92.7%
LR-T9	4800	0.6	1.46E-02	3	4.38E-02	8.42	0.0%	12.6%	22.5%	31.0%	47.6%	75.2%	88.5%	93.3%

Notes:

- The results for Tests LR-T2 and LR-T3 (shaded) were likely influenced by a developing GC-MS instrumental problem that was subsequently rectified. These tests were repeated as Tests LR-T3R and LR-T3A.
- The results for Test LR-T3R are from a re-analysis of samples from Test LR-T3.
- Test LR-T3A is a repeat of Test LR-T3 (repeated test and analysis).

Table 4.2. Acetamide Destruction Results from Large Reactor Tests with Steam Stripping Simulant and Acetamide.

Test	Lamp Power, W	Acetamide Concentration		$S_2O_8^{2-}$ to Acetamide Mole Ratio	$S_2O_8^{2-}$ Concentration		Acetamide Destruction vs. Time (minutes)							
		g/L	mol/L		mol/L	g/L	0	1	2	3	5	10	15	30
LR-T4	4800	0.86	1.46E-02	1.5	2.19E-02	4.21	0.0%	2.1%	41.1%	51.0%	39.0%	78.9%	66.9%	68.1%
LR-T5	4800	0.86	1.46E-02	1.5	2.19E-02	4.21	0.0%	4.0%	33.5%	39.4%	73.8%	66.4%	69.7%	79.9%
LR-T10	4800	0.86	1.46E-02	3	4.38E-02	8.42	0.0%	18.3%	36.1%	63.1%	75.7%	91.1%	97.2%	99.5%
LR-T11	4800	0.86	1.46E-02	3	4.38E-02	8.42	0.0%	22.2%	48.1%	57.8%	78.3%	90.1%	97.1%	99.2%

Table 4.3. Acetate Destruction Results from Large Reactor Tests with Steam Stripping Simulant and Acetate.

Test	Lamp Power, W	Acetate Concentration		$S_2O_8^{2-}$ to Acetate Mole Ratio	$S_2O_8^{2-}$ Concentration		Acetate Destruction vs. Time (minutes)							
		g/L	mol/L		mol/L	g/L	0	1	2	3	5	10	15	30
LR-T6	4800	0.86	1.46E-02	1.5	2.19E-02	4.21	0.0%	31.3%	50.5%	52.8%	57.6%	64.4%	96.9%	97.5%
LR-T7	4800	0.86	1.46E-02	1.5	2.19E-02	4.21	0.0%	31.0%	50.4%	52.6%	57.5%	64.3%	97.0%	97.4%
LR-T12	4800	0.86	1.46E-02	3	4.38E-02	8.42	0.0%	47.7%	52.9%	59.1%	67.9%	96.8%	96.2%	95.4%
LR-T13	4800	0.86	1.46E-02	3	4.38E-02	8.42	0.0%	42.3%	48.0%	54.2%	63.9%	96.8%	96.1%	95.8%

Table 4.4. Acetamide Formation Results from Large Reactor Tests with Steam Stripping Simulant and Acetonitrile.

Test	Lamp Power, W	Acetonitrile Concentration		$S_2O_8^{2-}$ to Acetonitrile Mole Ratio	$S_2O_8^{2-}$ Concentration		Acetamide ***Formation**** vs. Time (minutes)							
		g/L	mol/L		mol/L	g/L	0	1	2	3	5	10	15	30
LR-T2	4800	0.6	1.46E-02	1.5	2.19E-02	4.21	< 0.1%	< 0.1%	< 0.1%	< 0.1%	< 0.1%	< 0.1%	< 0.1%	< 0.1%
LR-T9	4800	0.6	1.46E-02	3	4.38E-02	8.42	< 0.1%	< 0.1%	< 0.1%	< 0.1%	< 0.1%	< 0.1%	< 0.1%	< 0.1%

* Based on 100% conversion of 0.6 g/L of acetonitrile yielding 0.86 g/L of acetamide and an acetamide detection limit of 0.85 mg/L.

Table 4.5. Acetate Formation Results from Large Reactor Tests with Steam Stripping Simulant and Acetonitrile.

Test	Lamp Power, W	Acetonitrile Concentration		$S_2O_8^{2-}$ to Acetonitrile Mole Ratio	$S_2O_8^{2-}$ Concentration		Acetate ***Formation**** vs. Time (minutes)							
		g/L	mol/L		mol/L	g/L	0	1	2	3	5	10	15	30
LR-T2	4800	0.6	1.46E-02	1.5	2.19E-02	4.21	0.0%	0.0%	0.2%	0.2%	1.6%	10.3%	16.6%	20.2%
LR-T9	4800	0.6	1.46E-02	3	4.38E-02	8.42	0.0%	0.0%	0.0%	3.3%	5.1%	8.6%	12.8%	15.7%

* Based on 100% conversion of 0.6 g/L of acetonitrile yielding 0.86 g/L of acetate.

Table 4.6. Sulfate Formation Results from Large Reactor Tests with Steam Stripping Simulant and Acetonitrile or Acetate.

Test	Lamp Power, W	Acetonitrile or Acetate Concentration		$S_2O_8^{2-}$ to Acetonitrile or Acetate Mole Ratio	$S_2O_8^{2-}$ Concentration		Sulfate ***Formation**** vs. Time (minutes)							
		g/L	mol/L		mol/L	g/L	0	1	2	3	5	10	15	30
LR-T2 Acetonitrile	4800	0.6	1.46E-02	1.5	2.19E-02	4.21	NA	NA	52.3%	67.9%	87.2%	93.9%	103.5%	121.8%
LR-T6 Acetate	4800	0.86	1.46E-02	1.5	2.19E-02	4.21	3.9%	21.2%	42.1%	58.3%	78.7%	104.7%	98.4%	98.1%
LR-T7 Acetate	4800	0.86	1.46E-02	1.5	2.19E-02	4.21	3.9%	20.6%	41.9%	57.3%	78.0%	104.8%	98.4%	99.1%
LR-T9 Acetonitrile	4800	0.6	1.46E-02	3	4.38E-02	8.42	NA	NA	37.9%	50.2%	63.4%	85.3%	107.7%	107.8%
LR-T12 Acetate	4800	0.86	1.46E-02	3	4.38E-02	8.42	4.3%	18.5%	31.0%	42.7%	60.0%	96.9%	111.2%	112.4%
LR-T13 Acetate	4800	0.86	1.46E-02	3	4.38E-02	8.42	4.4%	19.0%	31.0%	42.0%	59.2%	96.3%	111.2%	111.3%

* Based on 100% conversion of 4.21 (8.42) g/L of persulfate ion yielding 4.21 (8.42) g/L of sulfate ion.

NA – Not analyzed.

Table 4.7. Initial and Final pH and Temperature Values for Each Test.

Test	Organic	$S_2O_8^{2-}$ to Organic Mole Ratio	Initial, t = 0 min		Final, T = 30 min	
			pH	Temperature, °C	pH	Temperature, °C
LR-T1	None	0	5.24	27.03	4.50	38.66
LR-T2	Acetonitrile	1.5	4.35	27.10	1.76	39.19
LR-T3, LR-T3R	Acetonitrile	1.5	3.66	27.04	1.77	39.10
LR-T3A	Acetonitrile	1.5	2.87	27.82	1.81	38.31
LR-T8	Acetonitrile	3	4.48	NA	1.59	NA
LR-T9	Acetonitrile	3	4.18	26.75	1.63	38.27
LR-T4	Acetamide	1.5	4.37	25.77	1.83	37.56
LR-T5	Acetamide	1.5	4.50	27.27	1.85	37.14
LR-T10	Acetamide	3	4.42	26.55	1.64	37.42
LR-T11	Acetamide	3	4.33	26.61	1.66	38.02
LR-T6	Acetate	1.5	6.87	26.14	2.07	37.44
LR-T7	Acetate	1.5	6.85	26.03	2.07	36.42
LR-T12	Acetate	3	6.85	26.57	1.74	37.09
LR-T13	Acetate	3	6.66	26.03	1.76	37.12

Table 5.1. Tests and Test Conditions for Data Sets Used for Modeling.

Test	Lamp Power, W	Acetonitrile Concentration		$S_2O_8^{2-}$ to Acetonitrile Mole Ratio	$S_2O_8^{2-}$ Concentration		Data Source
		g/L	mol/L		mol/L	g/L	
LR-S1	450	60	1.46E+00	1.5	2.19E+00	421	[7]
LR-S2	450	6	1.46E-01	1.5	2.19E-01	42.1	[7]
LR-S3	450	6	1.46E-01	3	4.38E-01	84.2	[7]
LR-S5	4800	6	1.46E-01	3	4.38E-01	84.2	[7]
LR-T3R	4800	0.6	1.46E-02	1.5	2.19E-02	4.21	This Work
LR-T3A	4800	0.6	1.46E-02	1.5	2.19E-02	4.21	This Work
LR-T8	4800	0.6	1.46E-02	3	4.38E-02	8.42	This Work
LR-T9	4800	0.6	1.46E-02	3	4.38E-02	8.42	This Work

Table 5.2. Parameters Used for Modeling; Large Reactor with Persulfate.

Parameter	Value	Units
φ	0.7	mol $S_2O_8^{2-}$/mol photon
ε @ 254 nm	22	liter/(mol cm)
I_0 @254 nm – 450 W	0.122	W/cm^2
I_0 @254 nm – 4800 W	1.65	W/cm^2
K @254 nm	2.124E-06	mol photon/Joule
R_1	3.75	cm
R_2	16.95	cm
Reflectivity Ratio, μ	0.4	None

Table 5.3. Extended Model Fitting Results for Large Reactor Tests with Persulfate.

Test	Lamp Power, W	Acetonitrile Concentration		$S_2O_8^{2-}$ to Acetonitrile Mole Ratio	$S_2O_8^{2-}$ Concentration		Data Source	Fitted k_1, L/(mol s)	Fitted $k_3[H_2O]$, 1/s
		g/L	mol/L		mol/L	g/L			
LR-S1	450	60	1.46E+00	1.5	2.19E+00	421	[7]	44.44	0*
LR-S2	450	6	1.46E-01	1.5	2.19E-01	42.1	[7]	0.3383	0.4080
LR-S3	450	6	1.46E-01	3	4.38E-01	84.2	[7]	10.53	43.90
LR-S5	4800	6	1.46E-01	3	4.38E-01	84.2	[7]	0.005245	0.01168
LR-T3R	4800	0.6	1.46E-02	1.5	2.19E-02	4.21	This Work	1.009	0.05369
LR-T3A	4800	0.6	1.46E-02	1.5	2.19E-02	4.21	This Work	0.7550	0.05264
LR-T8	4800	0.6	1.46E-02	3	4.38E-02	8.42	This Work	0.2413	0.03115
LR-T9	4800	0.6	1.46E-02	3	4.38E-02	8.42	This Work	0.2272	0.02756
Global Fit (all eight tests)								0.3851	0.04166

* Very flat minimum and poor convergence.

Table 6.1. Operating Parameters for the ETF Reverse Osmosis System [8].

Parameter	**Value**
Membrane Type	DuPont FilmTec BW30-8040 365
Temperature	Range: 50 – 90 °F Normal Value: 86 °F
pH	Range 4 – 7 Normal Value: 5
Feed Flow Rate	165 – 175 gpm
Inlet Pressure (RO Unit 1)	Range: 100 – 270 psig Normal Value: 120 – 140 psig
Inlet Pressure (RO Unit 2)	Range: 100 – 450 psig Normal Value: 190 – 215 psig
Permeate Pressure (RO Unit 1)	Range: <10 – 15 psig Normal Value: 7 – 15 psig
Permeate Pressure (RO Unit 2)	Range: 100 – 270 psig Normal Value: 100 – 115 psig
Brine Pressure (RO Unit 2)	Range: 50 – 80 psig Normal Value: 50 – 57 psig

Table 6.2. Comparison of RO Elements for ETF System and VSL Test System. Data are from [32].

Parameter	**BW30-8040-365 (ETF)**	**BW30-2540-43 (VSL)**
Element Diameter, in.	8.0	2.5
Element Length, in.	40	40
Active Membrane Area (A), ft^2 (m^2)	365 (33.9)	43 (4.0)
Max. Feed Rate (F_{max}), m^3/h	12	1.4
Max. Permeate Rate (P_{max}), m^3/h	0.93	0.063
Min. Concentrate Rate (C_{min}), m^3/h	3.6	0.23
Nom. Design Flux (*f*), lmh*	19	19
Nom. Inlet Pressure (P_f), psig (barg)	130 (9.0)	130 (9.0)
Nom. Feed Rate (F)**, m^3/h (lpm)	5.81 (96.9)	0.684 (11.4)
Max. Feed-Concentrate Pressure Drop, psid	15	15

* $l/h/m^2/barg$

** $F = f \cdot A \cdot P_f$

Table 6.3. Simulant Composition for Reverse Osmosis Testing.
Data are from gPROMS Run 3 in [33].

Component	Concentration (mg/L)
Na^+	359
NH_4^+	36.8
SO_4^{2-}	807
NO_3^-	20.0
NO_2^-	9.22
Cl^-	1.52
HCO_3^-	0.454*

Simulant was spiked with organics listed in Table 6.4.
Simulant was charge balanced and adjusted to pH 5.0 +/- 0.2 by addition of sulfuric acid.
* This value will vary with pH, temperature, and CO_2 fugacity due to decomposition and release of CO_2.

Table 6.4. Organics Concentrations in Simulant for Reverse Osmosis Testing and Data from gPROMS Run 3 in [33].

Constituent	CAS Number	MW	gPROMS Concentrations (mg/l)	Simulant Concentrations (mg/L)
Acetonitrile	75-05-8	41.05	176	176
Acetone	67-64-1	58.08	0.0641	1.00*
Acrylonitrile	107-13-1	53.06	0.218	0.218
n-Nitrosodimethylamine (NDMA)	62-75-9	74.08	0.0222	0.0222
Acetate	64-19-7	60.05	1.66	1.66
Formate	64-18-6	46.03	0.206	1.66*

* Increased from gPROMS Run 3 value per WRPS direction.

Table 6.5. Average, Maximum, and Minimum Values for the Electronically Recorded Data During Each Day of Testing.

-	**Date**	**8/2/2021**			**8/3/2021**			**8/4/2021**			**8/5/2021**			**8/6/2021**		
-	Run time (hr)	8.1			8.0			8.0			8.0			8.0		
-	-	Avg.	Max.	Min.	Avg.	Max.	Min.	Avg.	Max.	Min.	Avg.	Max.	Min.	Avg.	Max.	Min.
Membrane 1	P_{F1} Inlet Pressure (psig)	133.0	145.7	116.3	132.5	141.6	126.0	132.6	142.4	124.9	132.6	144.2	124.5	132.6	143.6	125.1
	P_{C1} Outlet Pressure (psig)	121.9	126.9	102.9	121.7	127.3	113.9	121.6	127.1	115.3	121.5	127.0	116.3	121.5	127.1	118.3
	Avg. Pressure drop (psi)	11.1	NA	NA	10.7	NA	NA	11.1	NA	NA	11.0	NA	NA	11.1	NA	NA
	Feed Flow* (lpm)	13.6	NA	NA	13.5	NA	NA	13.4	NA	NA	13.4	NA	NA	13.4	NA	NA
	F_{P1} Permeate Flow (lpm)	1.13	1.18	1.00	1.10	1.14	0.97	1.08	1.12	0.16	1.07	1.10	0.91	1.06	1.09	0.66
	Recovery (%)**	8.3	NA	NA	8.2	NA	NA	8.1	NA	NA	8.0	NA	NA	7.9	NA	NA
Membrane 2	P_{F2} Inlet Pressure (psig)	130.2	139.7	125.8	129.6	135.5	108.8	129.3	137.9	124.7	129.3	135.2	124.8	128.9	135.4	97.2
	P_{C2} Outlet Pressure (psig)	118.8	126.4	115.1	118.4	125.1	98.2	118.2	124.3	114.6	118.1	122.3	114.6	117.7	122.9	87.1
	Avg. Pressure drop (psi)	11.3	NA	NA	11.2	NA	NA	11.2	NA	NA	11.1	NA	NA	11.2	NA	NA
	Feed Flow* (lpm)	12.5	NA	NA	12.4	NA	NA	12.4	NA	NA	12.4	NA	NA	12.4	NA	NA
	F_{P2} Permeate Flow (lpm)	1.00	1.05	0.05	0.97	1.02	0.24	0.96	1.02	0.12	0.94	0.99	0.57	0.94	1.01	0.67
	Recovery (%)**	8.0	NA	NA	7.8	NA	NA	7.7	NA	NA	7.6	NA	NA	7.6	NA	NA
	F_c Concentrate Flow (lpm)	11.5	11.9	11.1	11.4	11.8	10.9	11.4	11.9	11.1	11.4	11.8	11.0	11.4	11.8	9.2
	Total Recovery (%)**	15.7	NA	NA	15.4	NA	NA	15.2	NA	NA	15.0	NA	NA	14.9	NA	NA

* For Membrane 1, the feed flow is the sum of Membrane 1 & 2 permeate and concentrate flow. For Membrane 2, the feed flow is the sum of the Membrane 2 permeate and concentrate flow.

** Recovery is defined here as the permeate flow divided by the feed flow expressed in percent. It is calculated here using average values.

NA – Not applicable

Table 6.5. Results from Organic Analysis of Samples from RO Tests.

-	Zero to 8 hours				8 to 16 hours			16 to 24 hours		
	Acetonitrile	**Acetone**	**Acrylonitrile**	**NDMA**	**Acetonitrile**	**Acetone**	**Acrylonitrile**	**Acetonitrile**	**Acetone**	**Acrylonitrile**
	Peak Areas Expressed as a Fraction of Feed									
Feed	100%	100%	100%	100%	100%	100%	100%	100%	100%	100%
Concentrate 1	94.3%	91.2%	90.3%	93.5%	98.5%	97.2%	92.3%	98.4%	86.1%	84.9%
Concentrate 2	94.8%	92.9%	87.8%	97.9%	97.8%	94.4%	95.3%	96.2%	80.9%	83.6%
Permeate 1	85.7%	36.8%	72.8%	37.1%	93.2%	39.9%	82.6%	92.5%	34.5%	73.0%
Permeate 2	81.7%	36.8%	68.1%	45.2%	92.8%	45.8%	93.5%	92.3%	35.8%	74.8%
	*Rejection Rate**									
Membrane 1	14.3%	63.2%	27.2%	62.9%	6.8%	60.1%	17.4%	7.5%	65.5%	27.0%
Membrane 2	13.4%	59.6%	24.5%	51.7%	5.8%	52.9%	-1.3%	6.2%	58.5%	11.9%

-	24 to 32 hours			24 to 32 hours (repeat)			32 to 40 hours			
	Acetonitrile	**Acetone**	**Acrylonitrile**	**Acetonitrile**	**Acetone**	**Acrylonitrile**	**Acetonitrile**	**Acetone**	**Acrylonitrile**	**NDMA**
	Peak Areas Expressed as a Fraction of Feed									
Feed	100%	100%	100%	100%	100%	100%	100%	100%	100%	100%
Concentrate 1	100%	102%	96.2%	101%	99%	98.1%	93.1%	78.0%	79.4%	101%
Concentrate 2	106%	103%	97.5%	100%	96%	98.7%	95.1%	75.8%	79.7%	103%
Permeate 1	89.8%	38.3%	81.6%	95.6%	38.6%	87.3%	78.0%	27.2%	57.7%	38%
Permeate 2	87.4%	43.8%	84.0%	93.2%	41.5%	85.4%	86.0%	34.3%	68.4%	44.5%
	*Rejection Rate**									
Membrane 1	10.2%	61.7%	18.4%	4.4%	61.4%	12.7%	22.0%	72.8%	42.3%	61.9%
Membrane 2	12.6%	56.9%	12.7%	7.4%	58.1%	13.0%	7.6%	56.0%	13.9%	56.0%

* Rejection Rate = (1 – permeate concentration/feed concentration) × 100

Table 6.6. Results from Organic Analysis of Samples from RO Tests Averaged Over All Sample Times.

-	Average Over All Sample Times			
	Acetonitrile	**Acetone**	**Acrylonitrile**	**NDMA**
	Peak Areas Expressed as a Fraction of Feed			
Feed	100%	100%	100%	100%
Concentrate 1	97.5%	92.2%	90.2%	97.3%
Concentrate 2	98.2%	90.4%	90.4%	100.7%
Permeate 1	89.1%	35.9%	75.8%	37.6%
Permeate 2	88.9%	39.7%	79.0%	44.8%
	Rejection Rate[*]			
Membrane 1	10.9%	64.1%	24.2%	62.4%
Membrane 2	8.8%	57.0%	12.4%	53.9%

* Rejection Rate = (1 – permeate concentration/feed concentration) × 100

Table 6.7. Results from Acetate and Formate Analysis of Samples from RO Tests.

Sample Location	Sample Time	Acetate + Formate Concentration, mg/L	Rejection Rate*
Permeate, Membrane 1	8 hours	0.29	91.4%
Permeate, Membrane 2		0.30	91.1%
Permeate, Membrane 1	16 hours	0.30	91.1%
Permeate, Membrane 2		0.30	91.1%
Permeate, Membrane 1	24 hours	0.34	89.9%
Permeate, Membrane 2		0.30	91.1%
Permeate, Membrane 1	32 hours	0.30	91.1%
Permeate, Membrane 2		0.33	90.2%
Permeate, Membrane 1	40 hours	0.31	90.8%
Permeate, Membrane 2		Not Measured	-
Permeate, Membrane 1	**Average**	0.31	90.9%
Permeate, Membrane 2		0.31	90.9%

* Rejection Rate = (1 – permeate concentration/feed concentration) × 100; calculated using the nominal feed concentrations in Table 6.4.

Table 6.8. Results from Sodium Analysis of Samples from RO Tests.

	45 min	**8 hrs**	**16 hrs**	**24 hrs**	**32 hrs**	**40 hrs**
	Sodium Concentration, mg/L					
Feed	347.9	347.9	365.0	352.0	342.4	348.0
Concentrate 1	318.1	355.5	353.0	355.8	351.7	357.2
Concentrate 2	322.2	361.2	370.2	374.7	372.5	371.6
Permeate 1	9.30	5.22	5.95	5.25	5.32	6.03
Permeate 2	9.81	5.46	6.62	4.96	5.51	5.63
	Rejection Rate[*]					
Membrane 1	97.3%	98.5%	98.4%	98.5%	98.4%	98.3%
Membrane 2	96.9%	98.5%	98.1%	98.6%	98.4%	98.4%

* Rejection Rate = (1 – permeate concentration/feed concentration) × 100

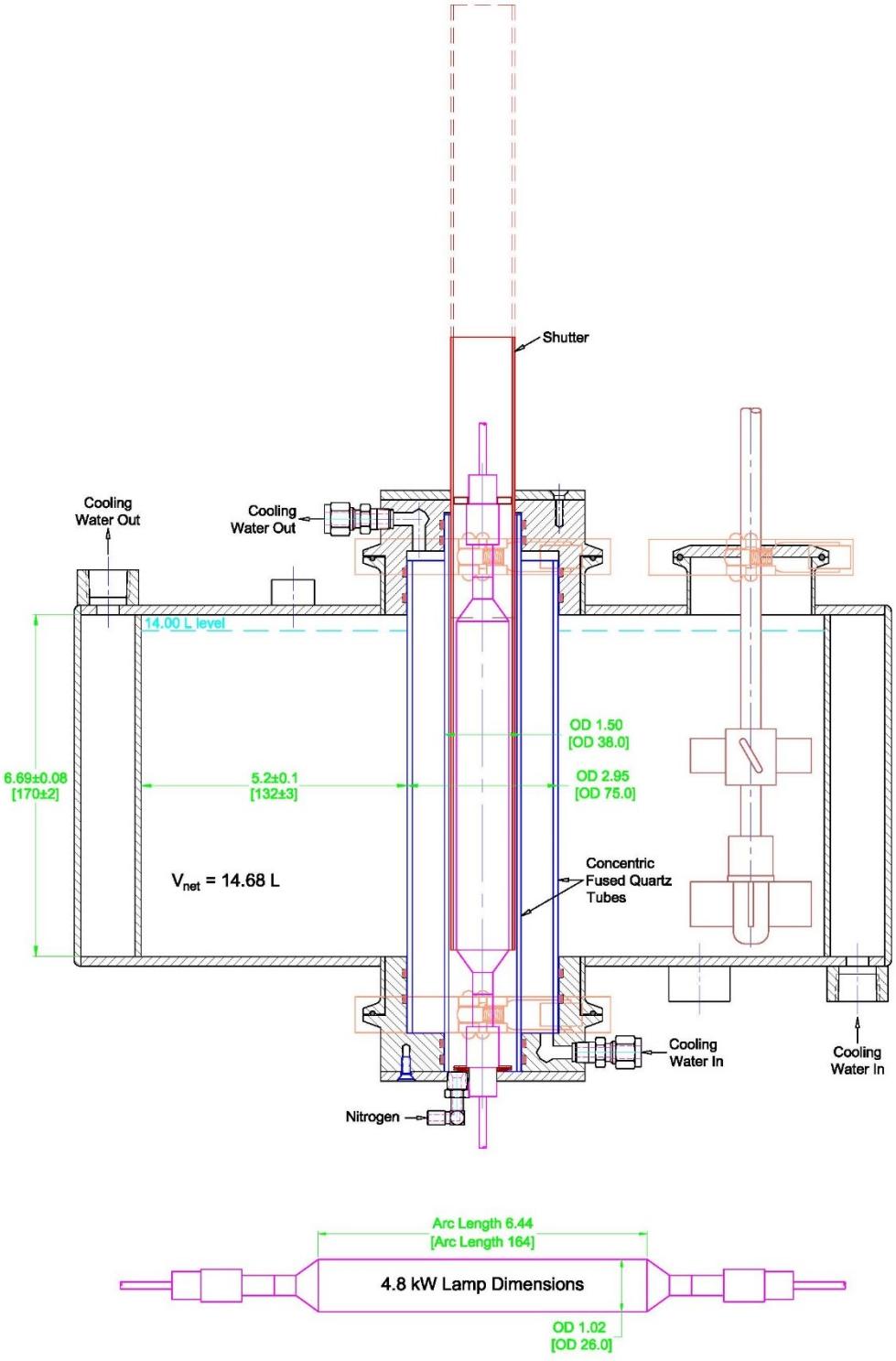

Figure 2.1. Cross-sectional diagram of the large reactor with the 4800 W UV lamp. Dimensions shown in inches and [millimeters].

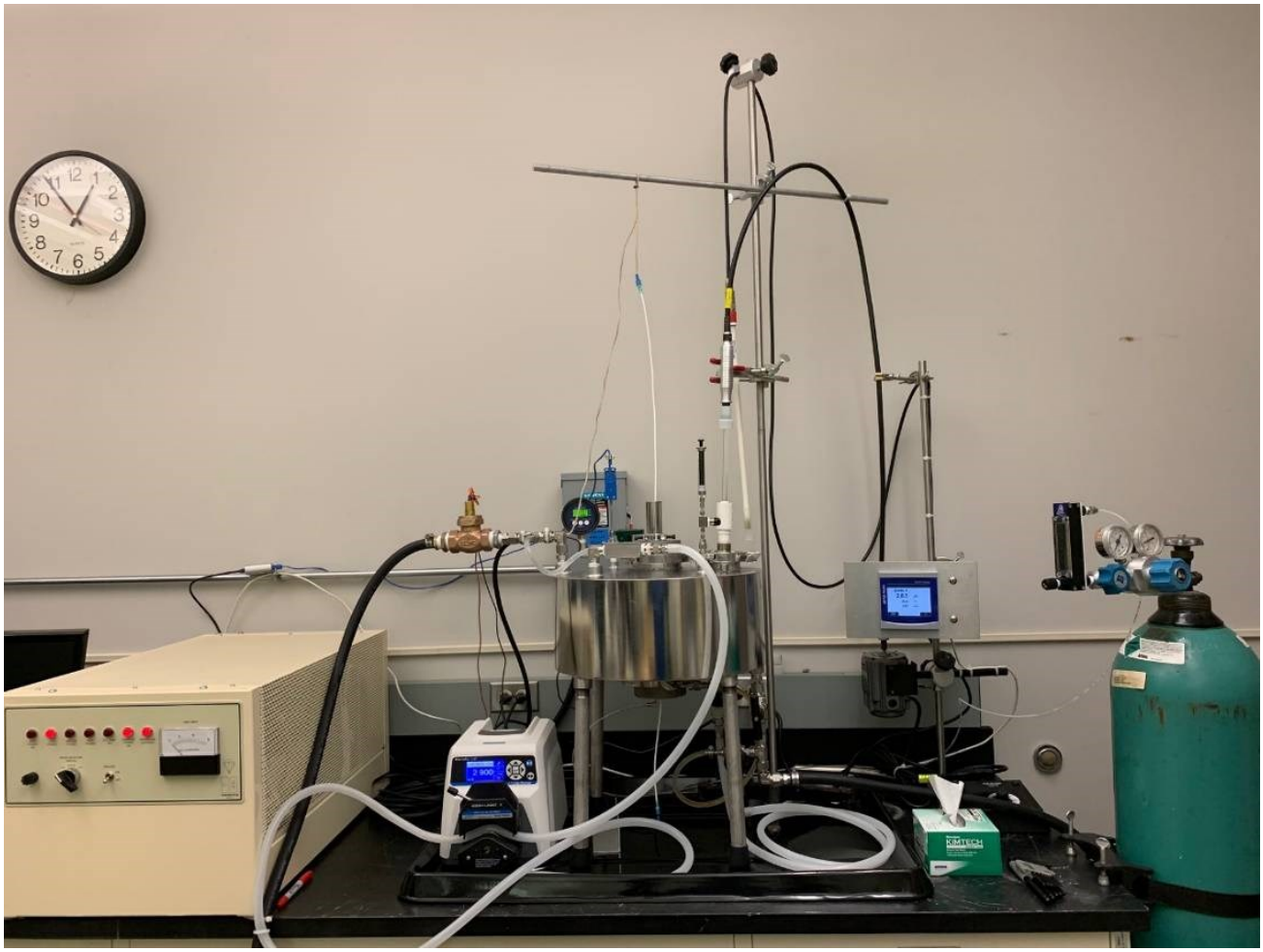

Figure 2.2. Large reactor setup with the 4800 W UV lamp. Lamp power supply is on the left.

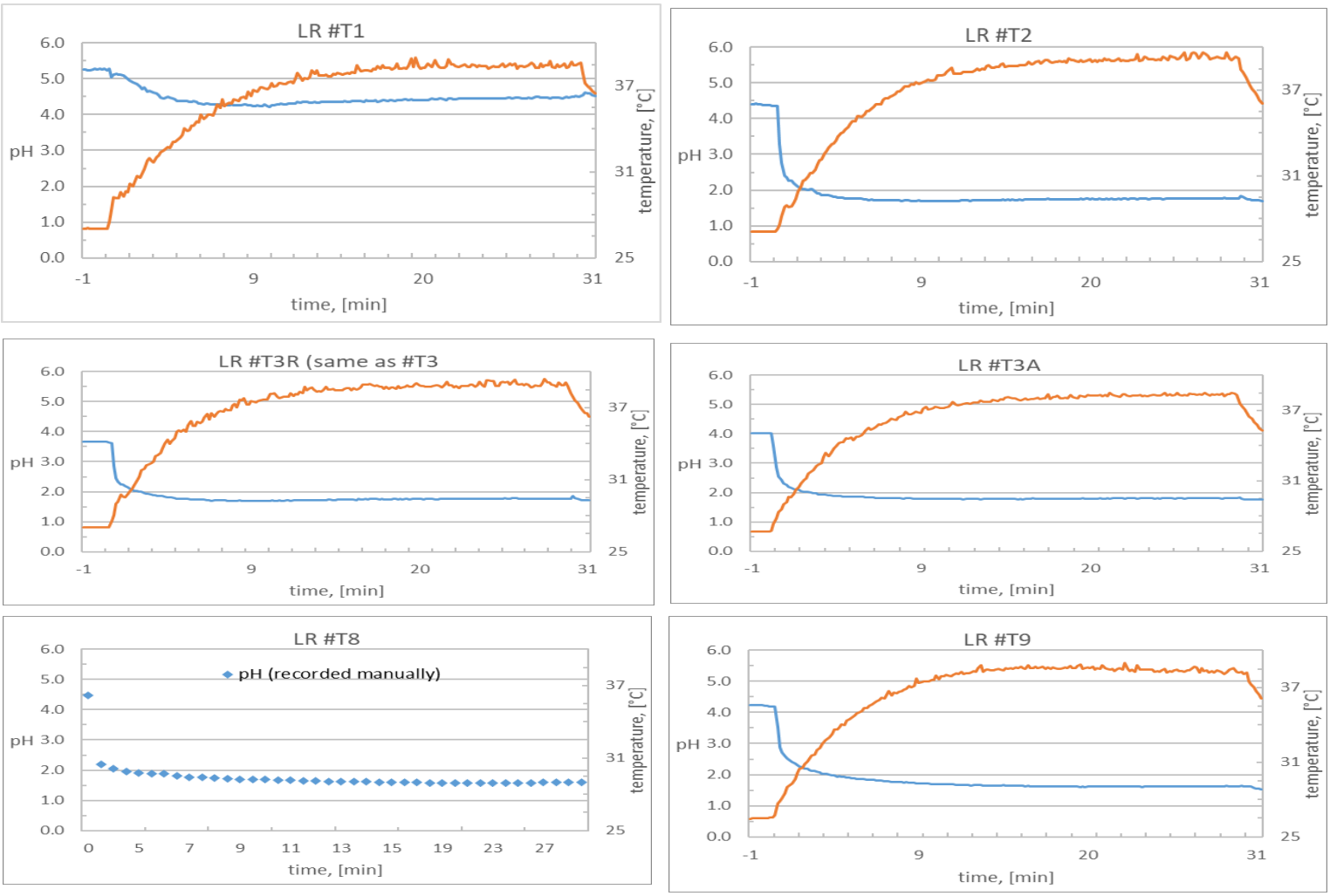

Figure 4.1. Temperature (red line) and pH (blue line) during large reactor tests with acetonitrile.

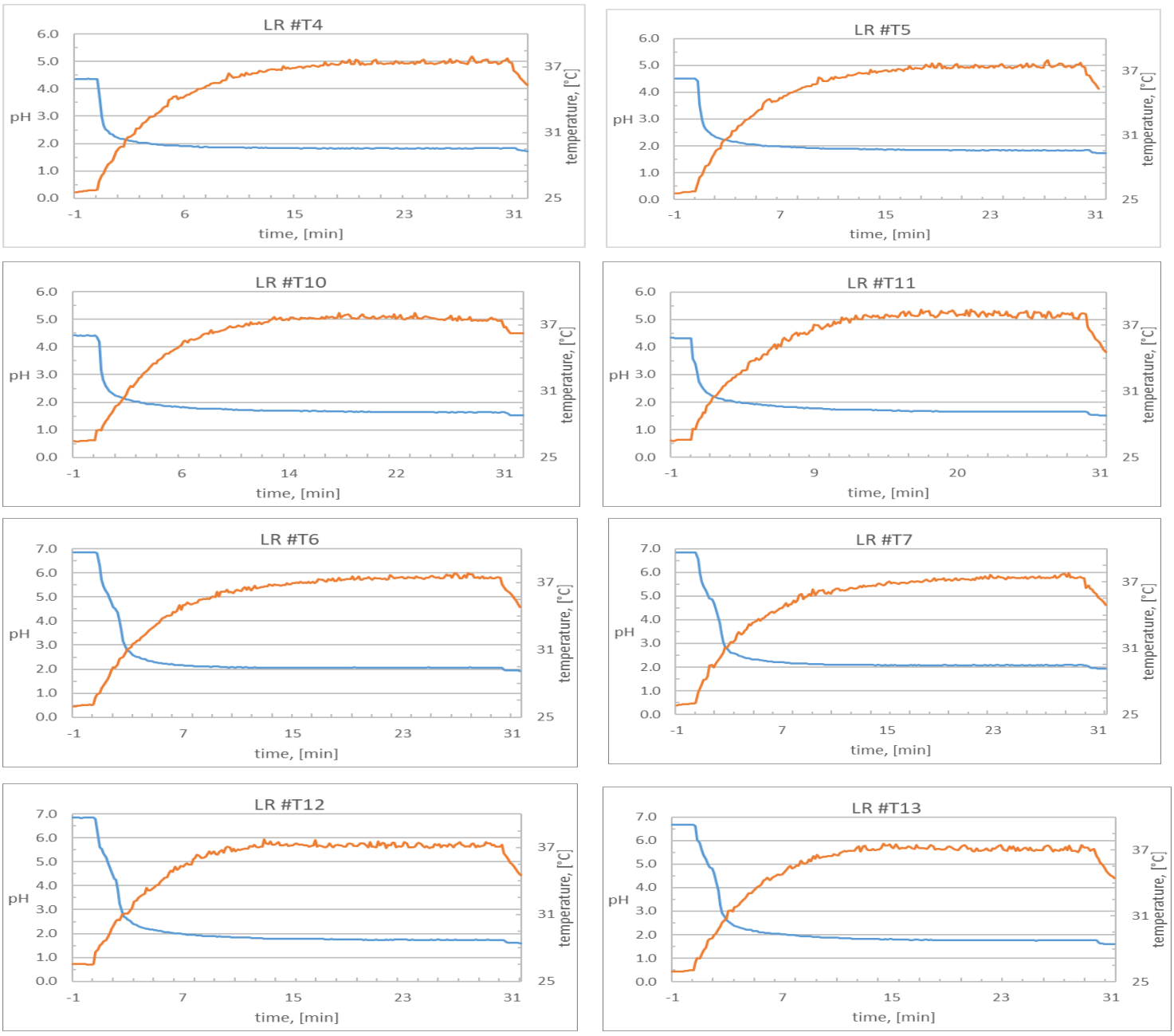

Figure 4.2. Temperature (red line) and pH (blue line) during large reactor tests with acetamide or acetate.

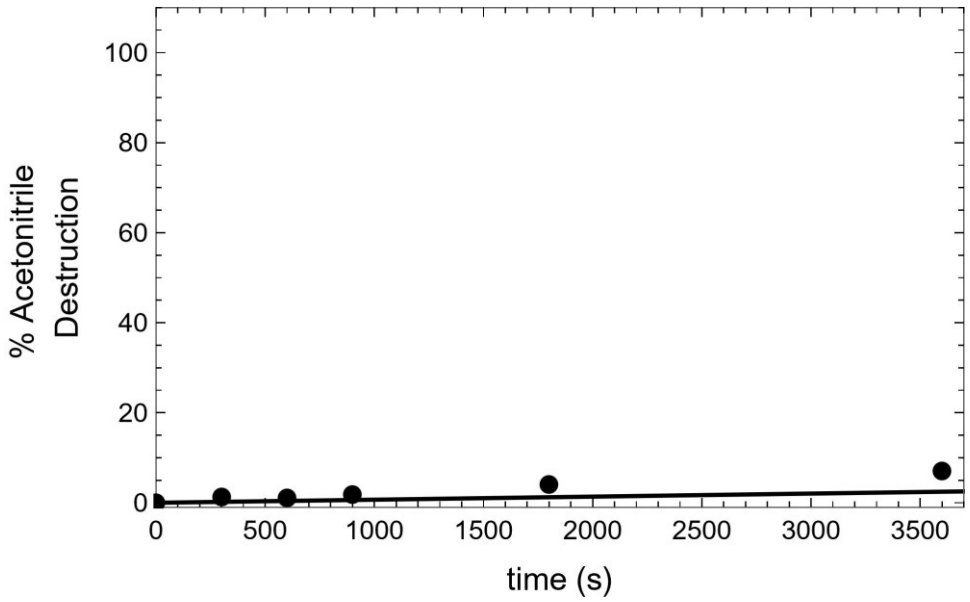

Figure 5.1. Extended model individual fit to the data from Test LR-S1.

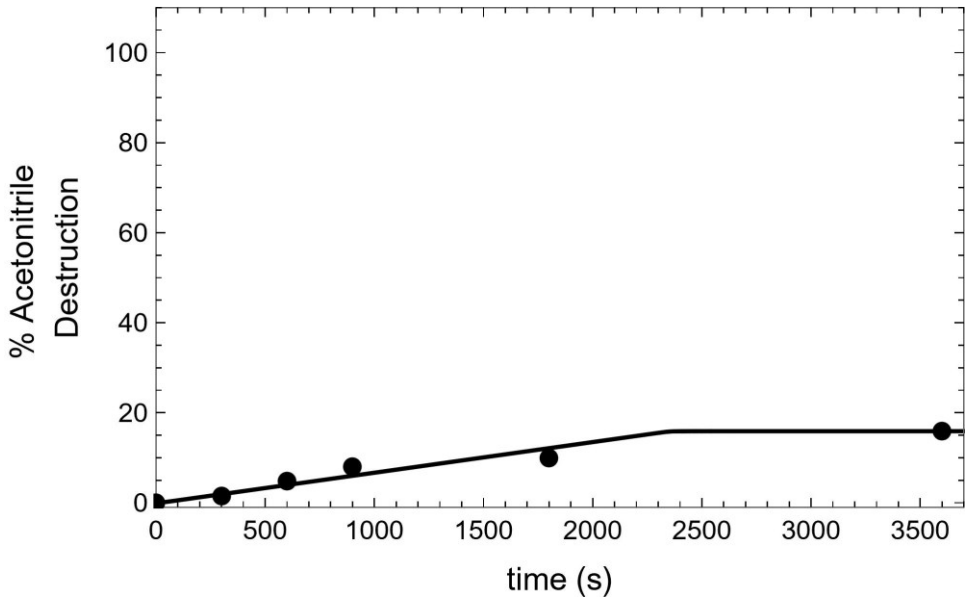

Figure 5.2. Extended model individual fit to the data from Test LR-S2.

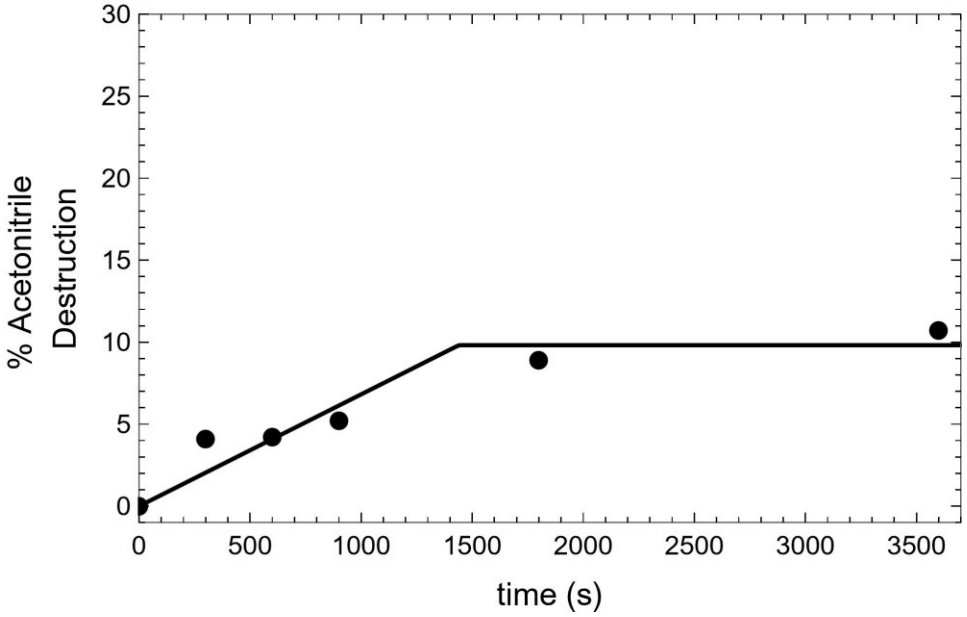

Figure 5.3. Extended model individual fit to the data from Test LR-S3.

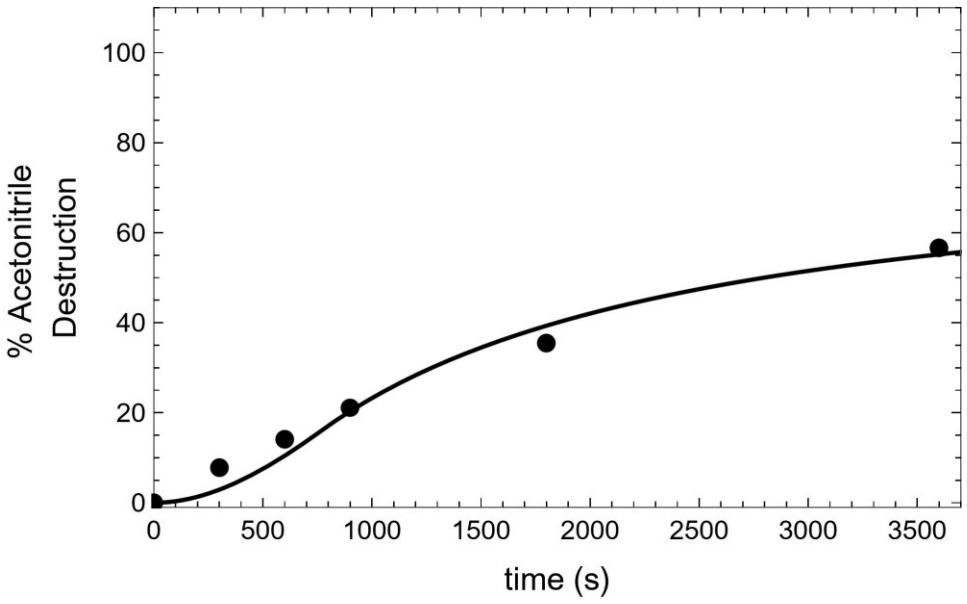

Figure 5.4. Extended model individual fit to the data from Test LR-S5.

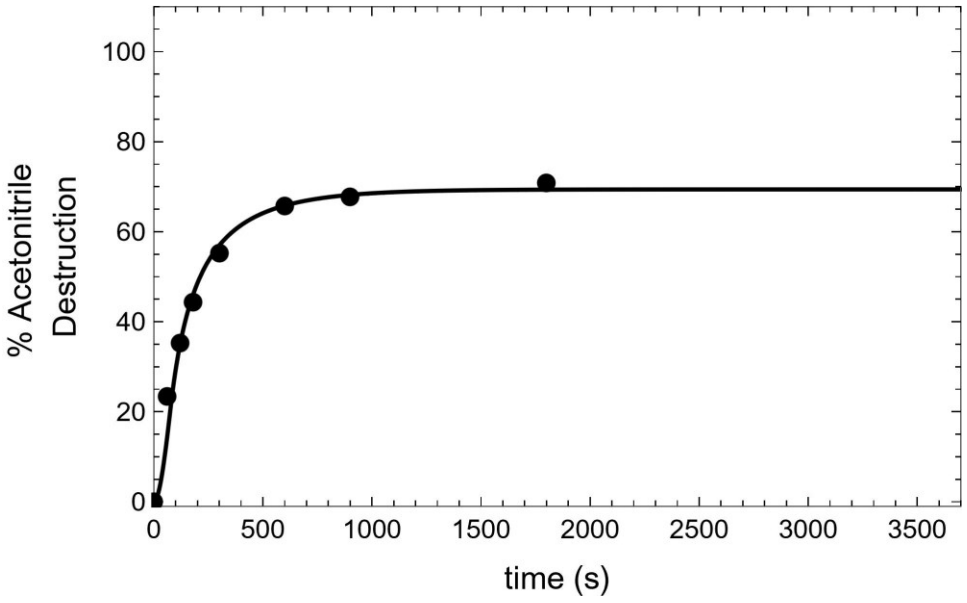

Figure 5.5. Extended model individual fit to the data from Test LR-T3A.

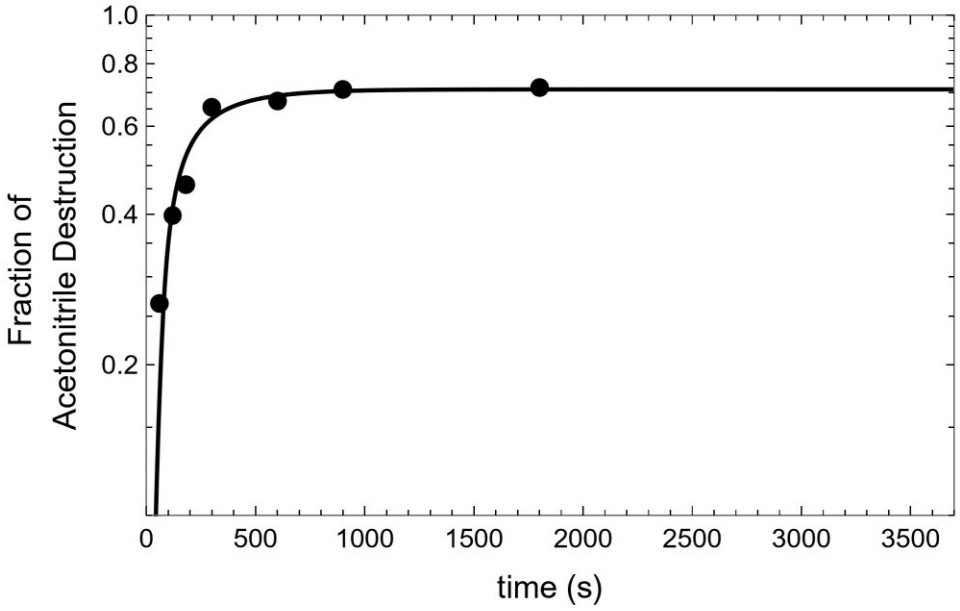

Figure 5.6. Extended model individual fit to the data from Test LR-T3R.

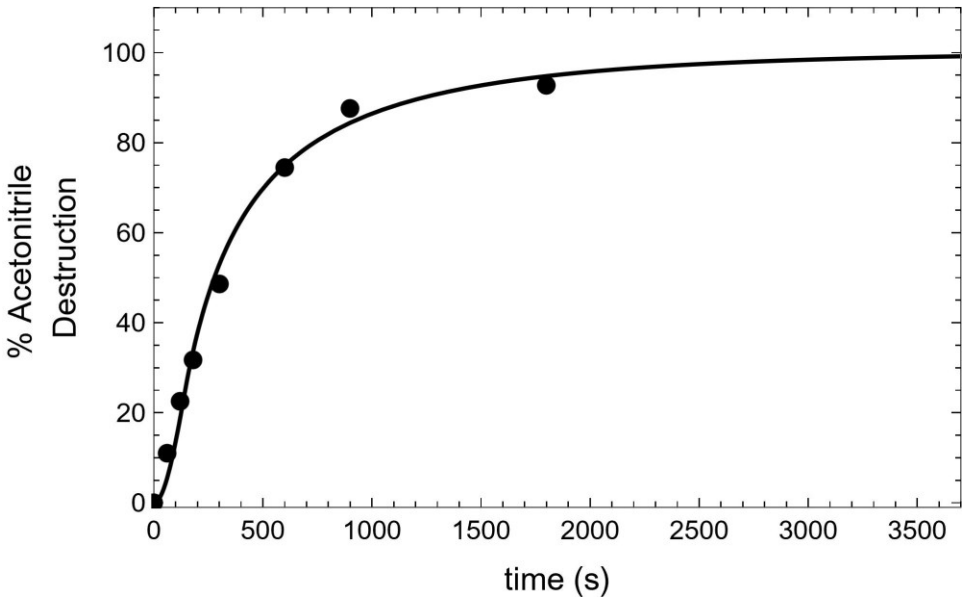

Figure 5.7. Extended model individual fit to the data from Test LR-T8.

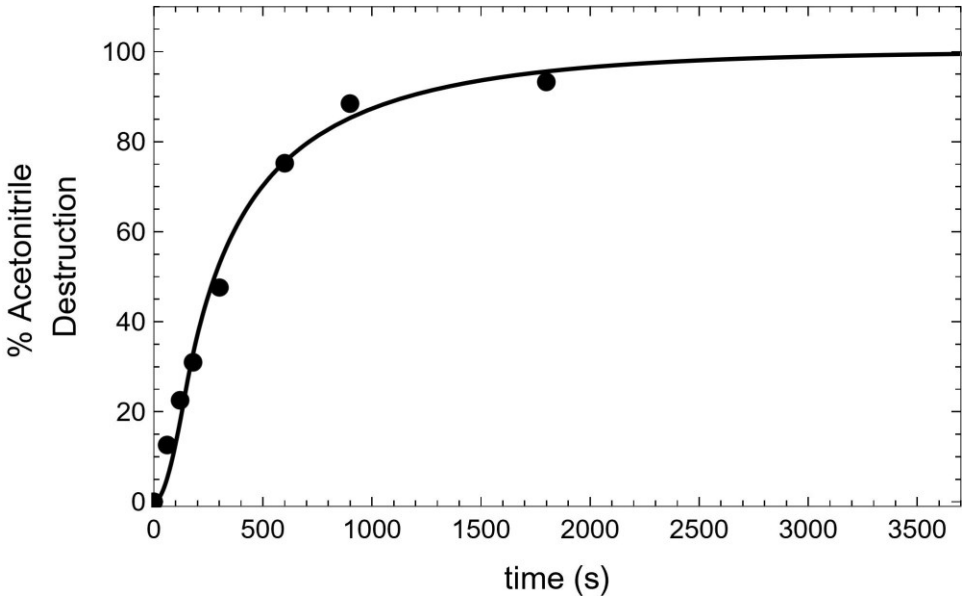

Figure 5.8. Extended model individual fit to the data from Test LR-T9.

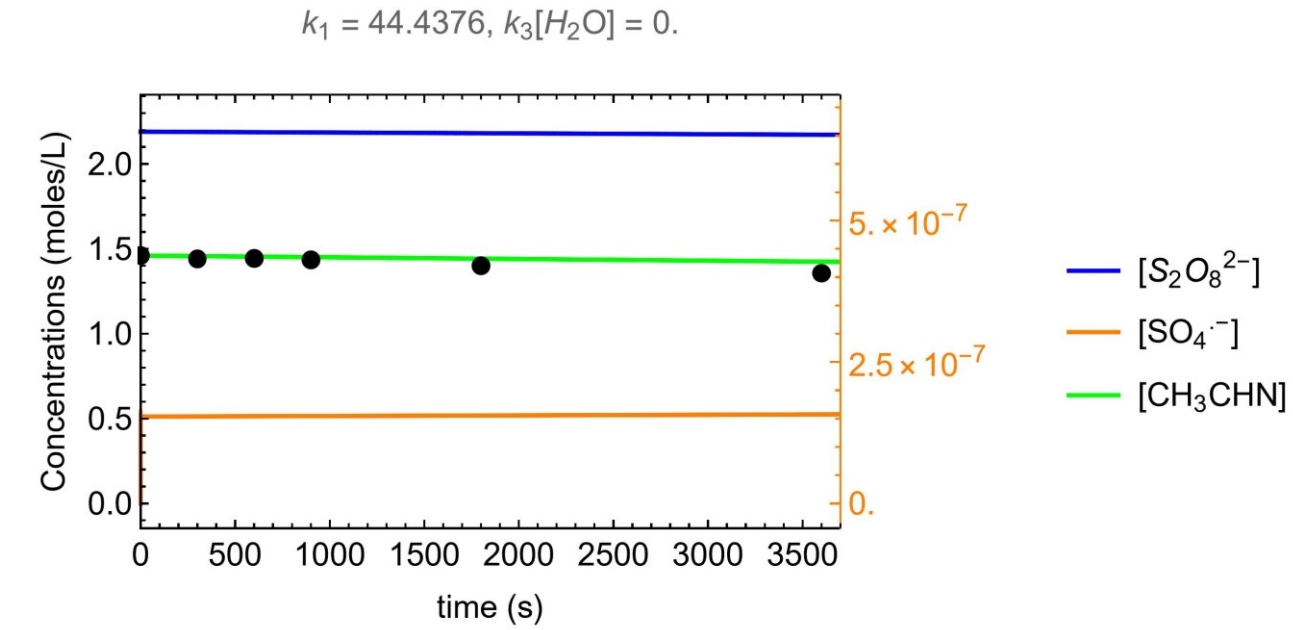

Figure 5.9. Extended model fit to Test LR-S1.

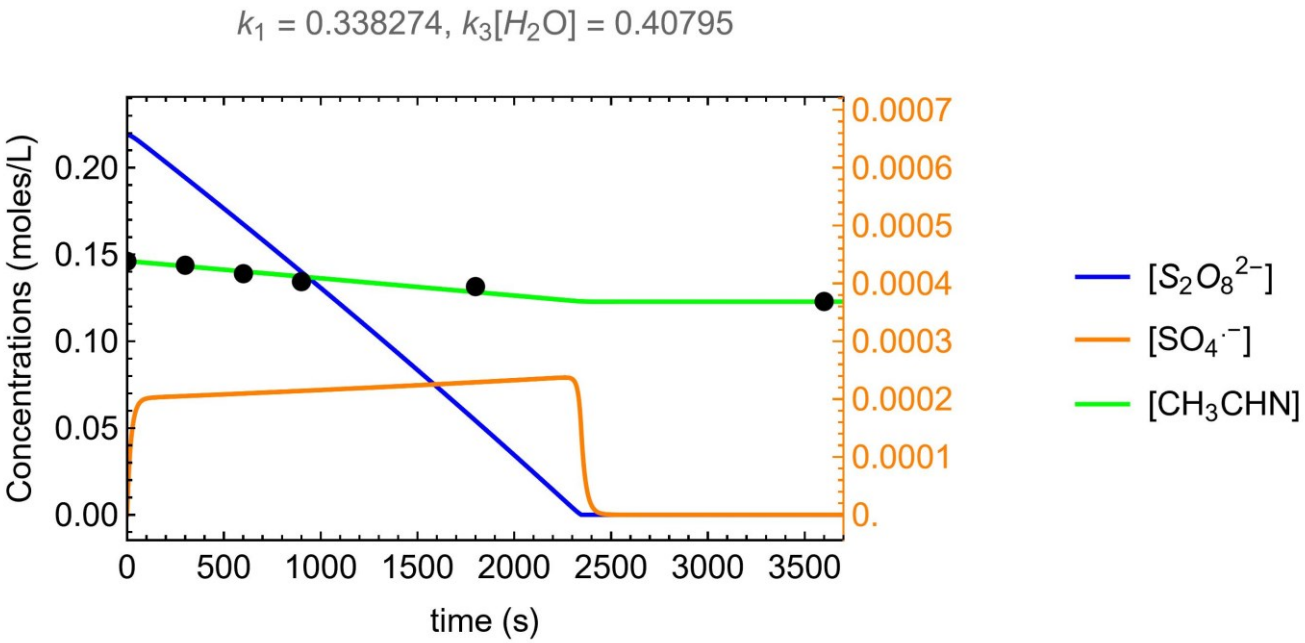

Figure 5.10. Extended model fit to Test LR-S2.

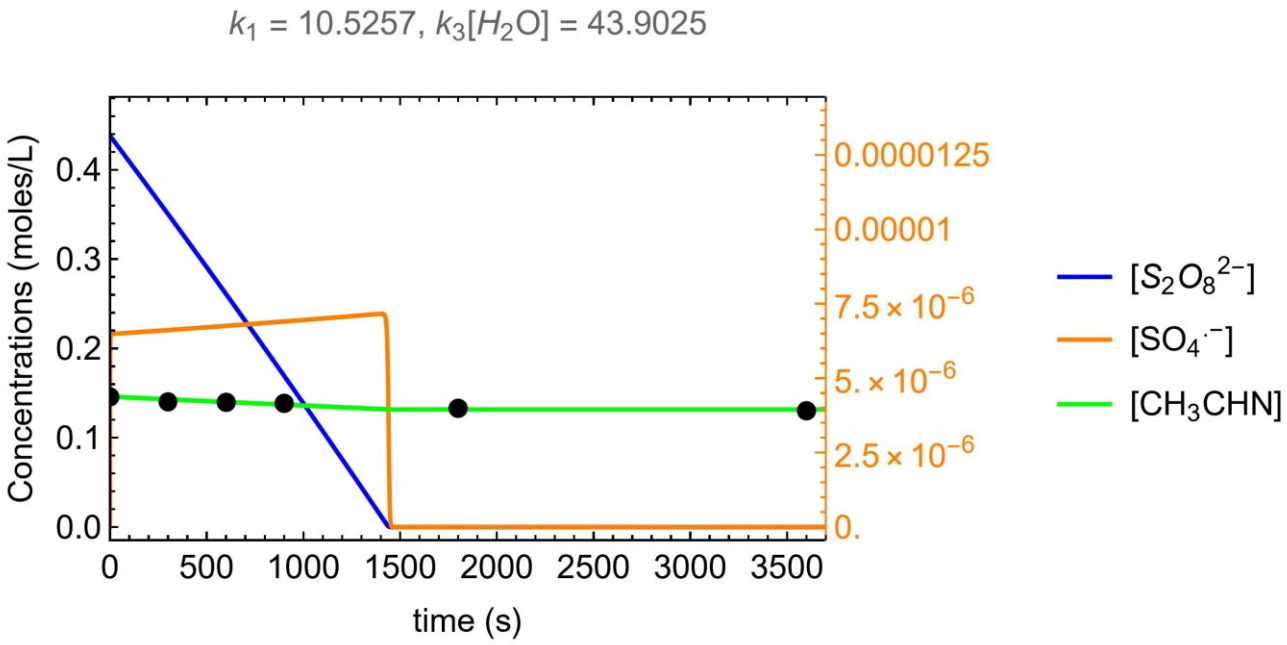

Figure 5.11. Extended model fit to Test LR-S3.

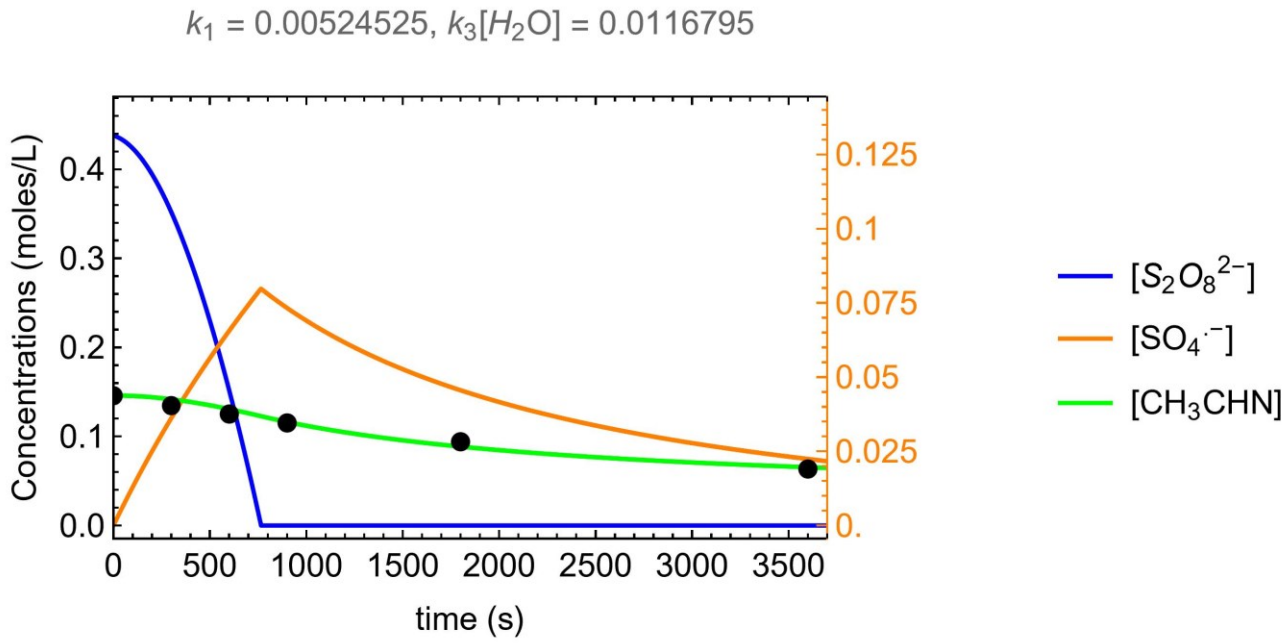

Figure 5.12. Extended model fit to Test LR-S5.

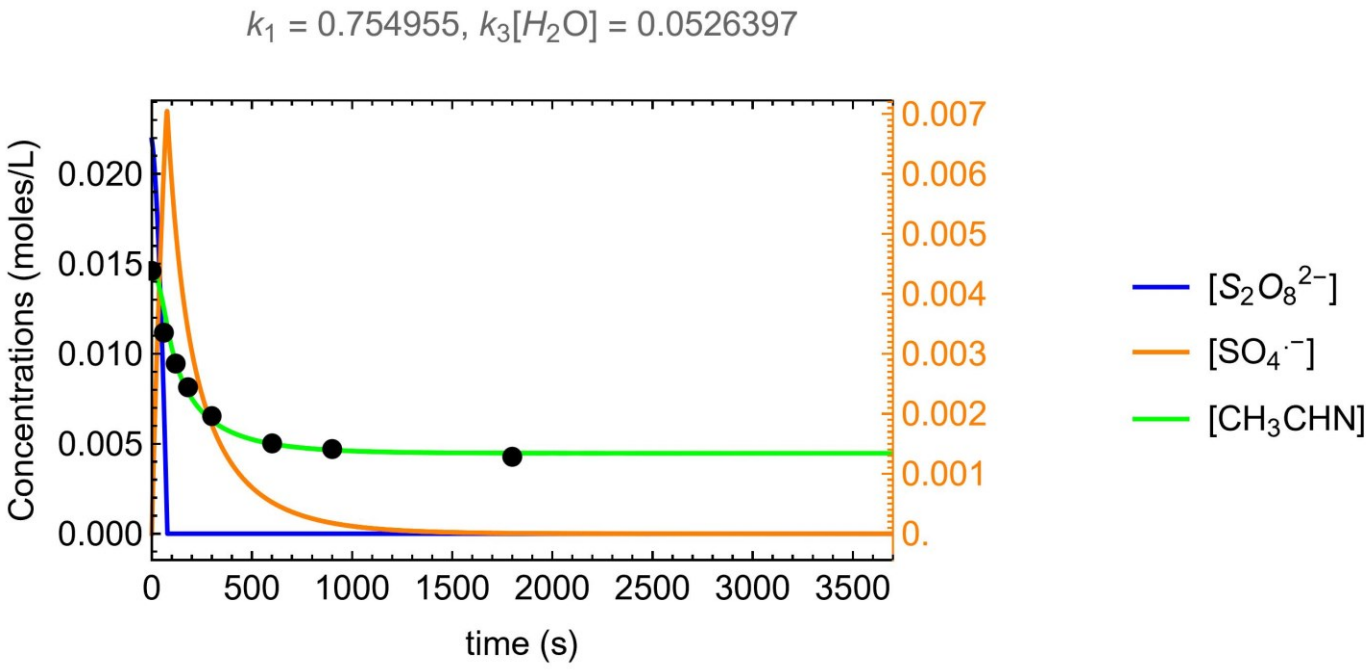

Figure 5.13. Extended model fit to Test LR-T3A.

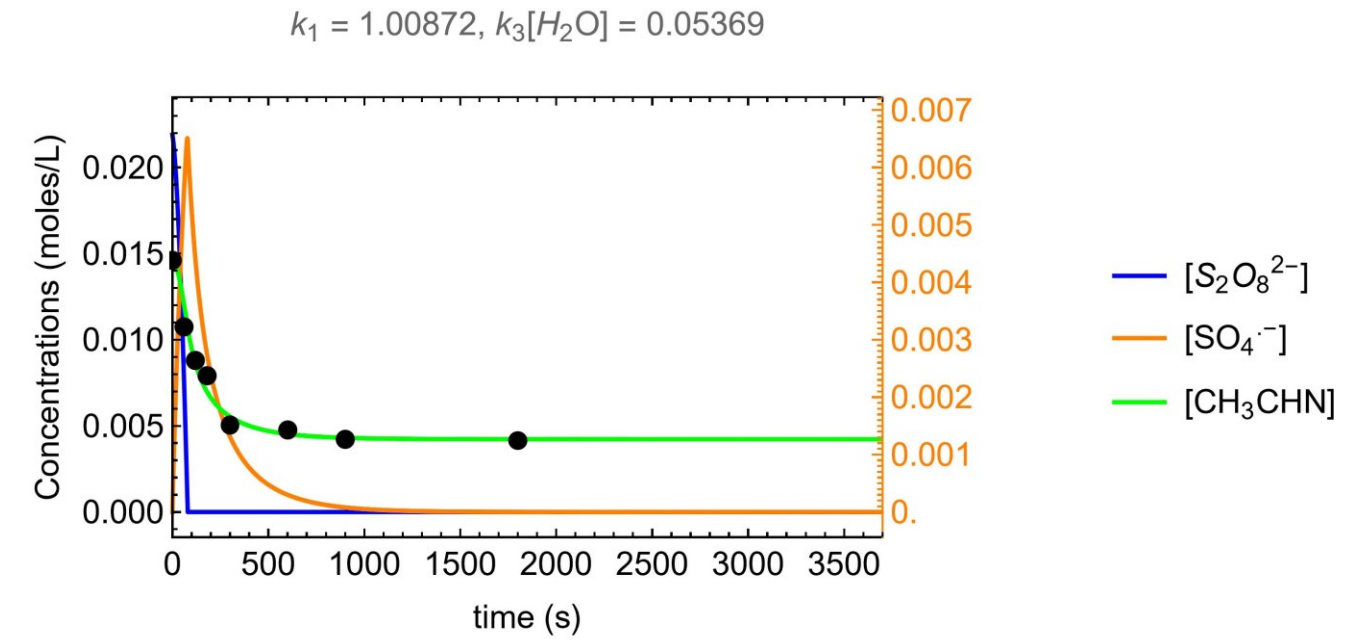

Figure 5.14. Extended model fit to Test LR-T3R.

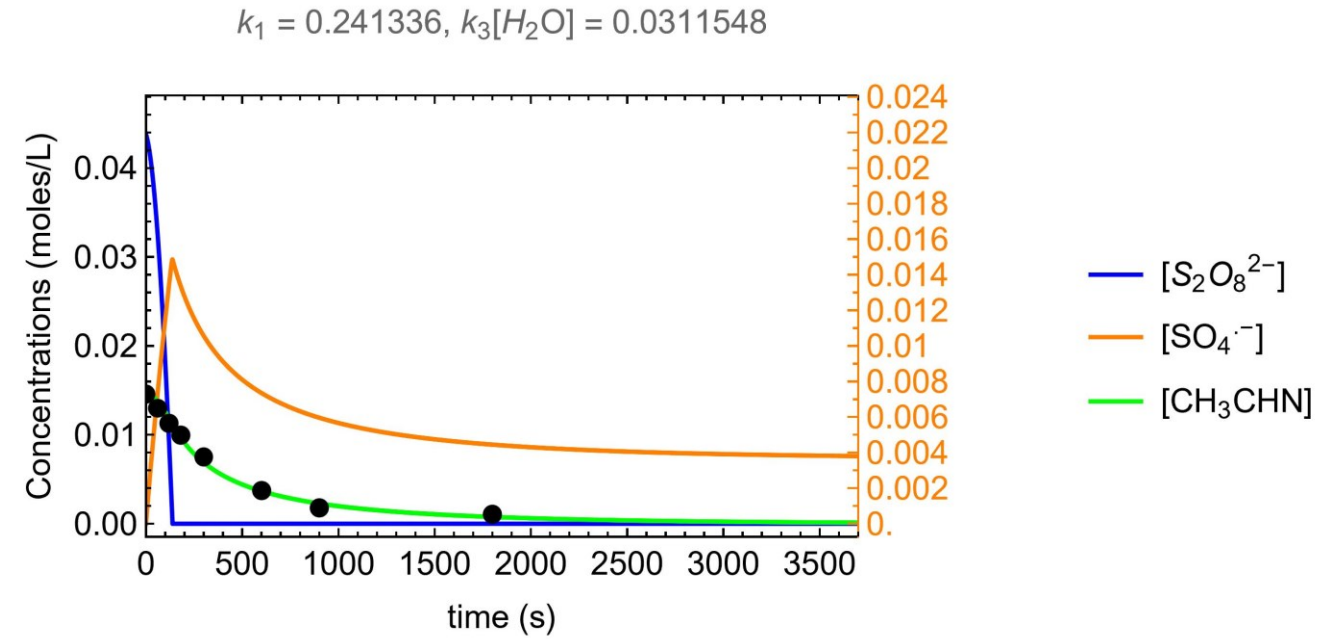

Figure 5.15. Extended model fit to Test LR-T8.

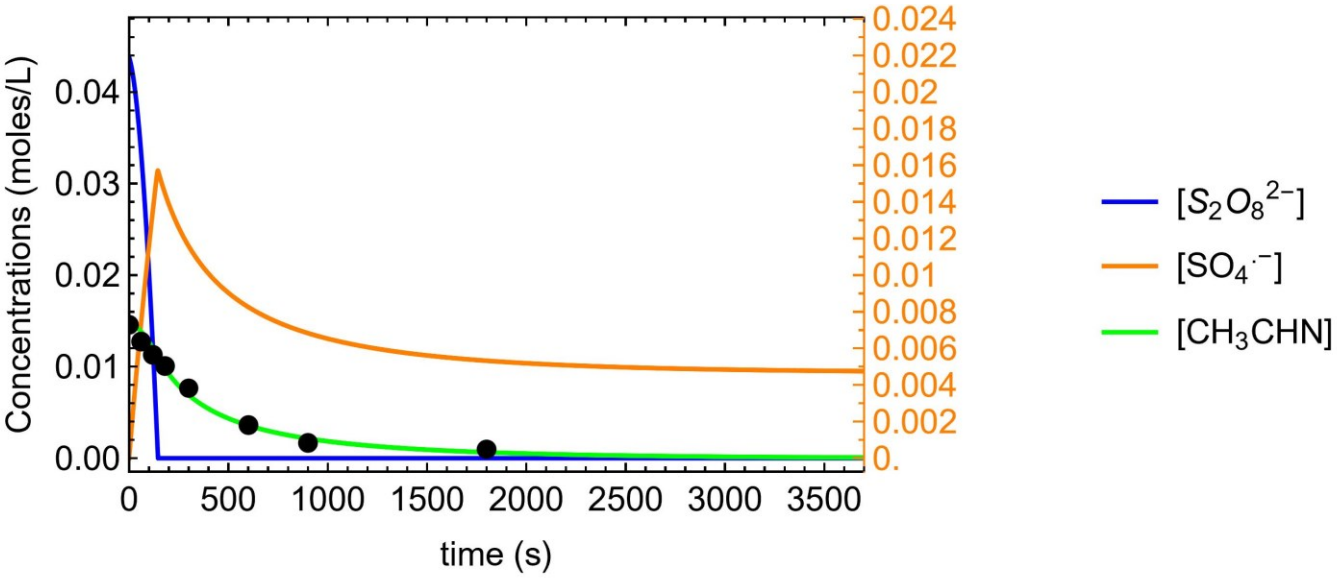

Figure 5.16. Extended model fit to Test LR-T9.

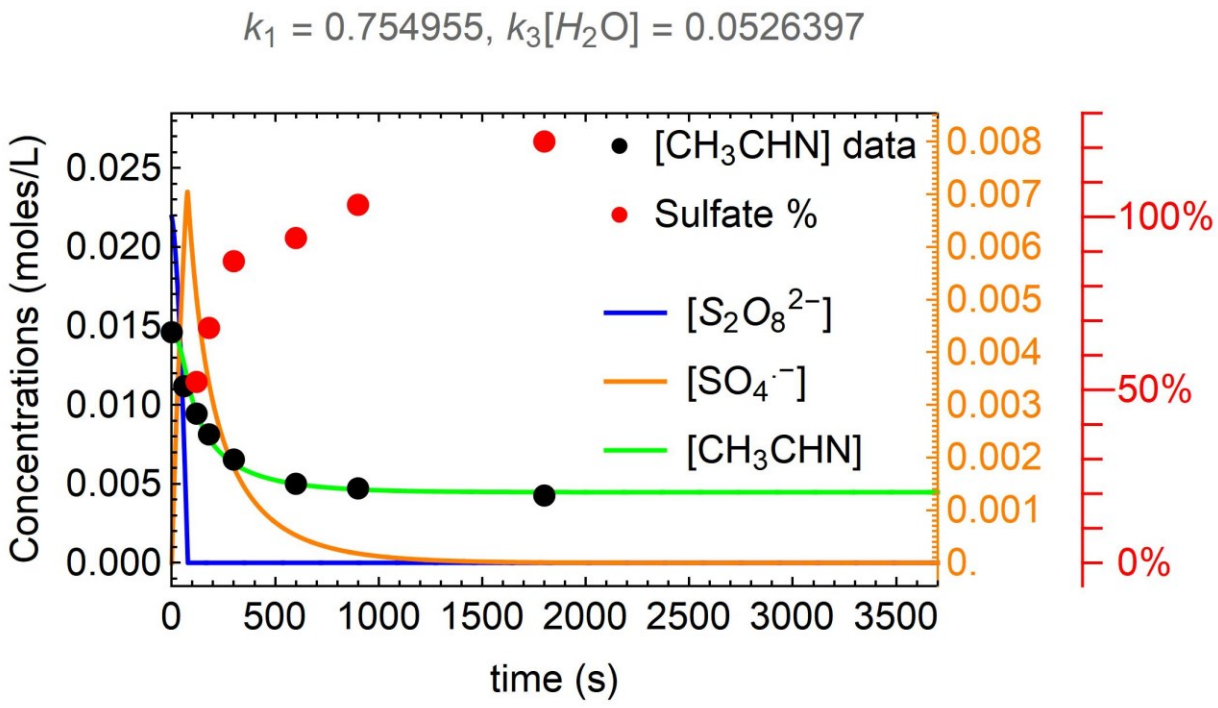

Figure 5.17. Extended model fit to Test LR-T3A shown in Figure 5.13 with measured sulfate data (as a percent of theoretical maximum) added for comparison.

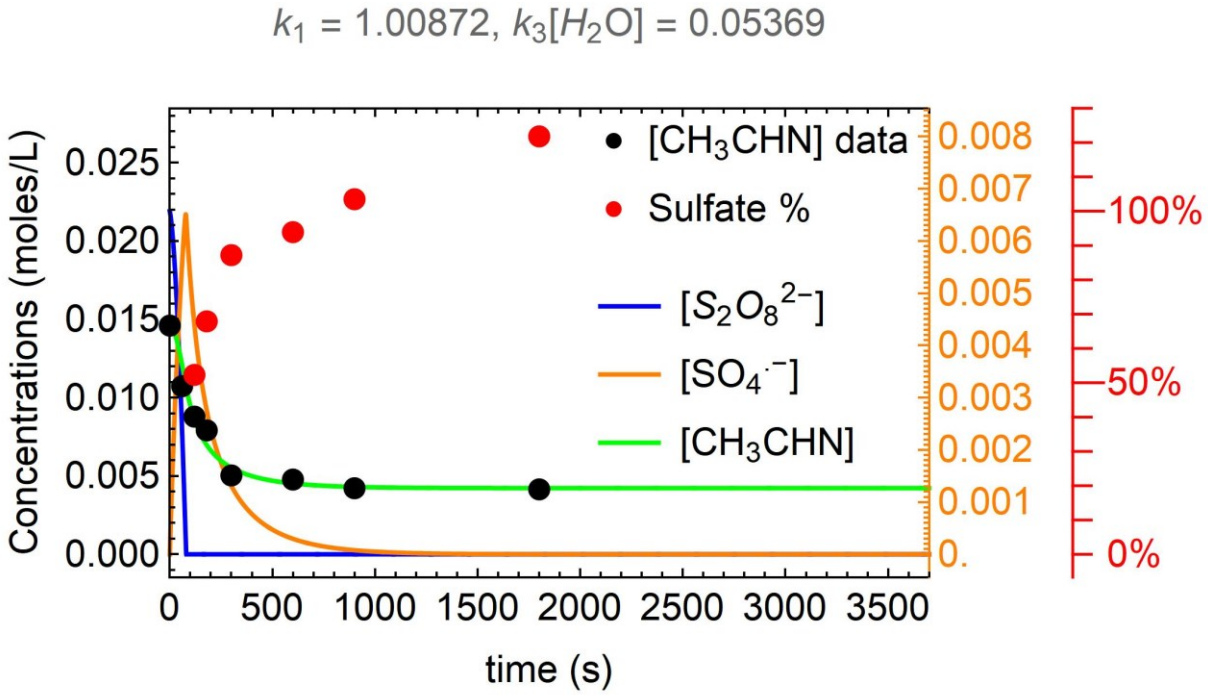

Figure 5.18. Extended model fit to Test LR-T3R shown in Figure 5.14 with measured sulfate data (as a percent of theoretical maximum) added for comparison.

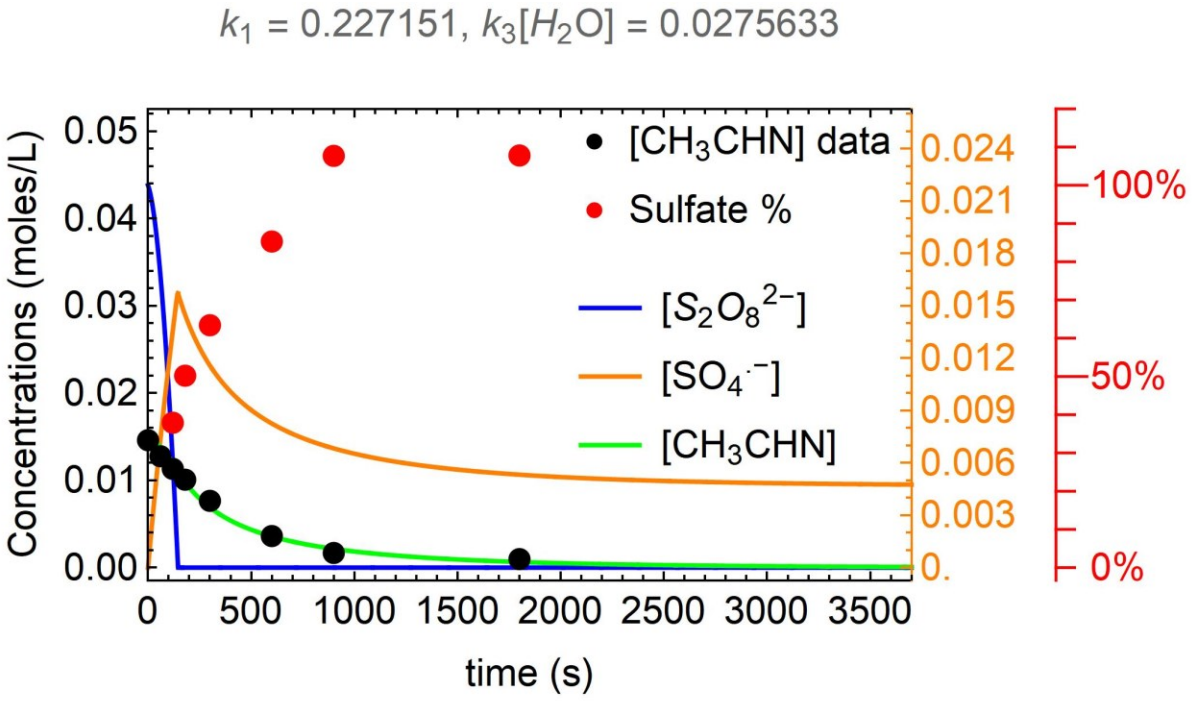

Figure 5.19. Extended model fit to Test LR-T9 shown in Figure 5.16 with measured sulfate data (as a percent of theoretical maximum) added for comparison.

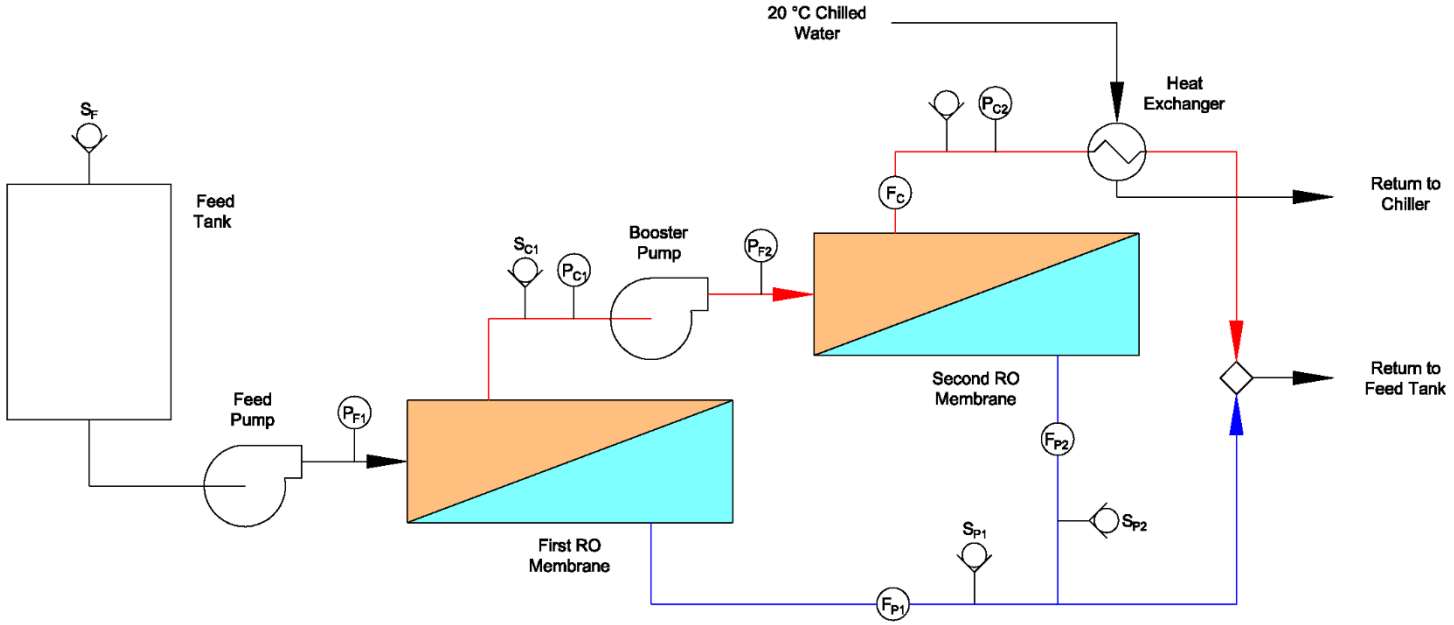

LEGEND:

P_{FX}	Membrane X Feed Pressure
P_{CX}	Membrane X Concentrate Pressure
F_{PX}	Membrane X Permeate Flow
F_C	Membrane 2 Concentrate Flow
S_F	Feed Tank Sample Port
S_{CX}	Membrane X Concentrate Sample Port
S_{PX}	Membrane X Permeate Sample Port

Figure 6.1. Schematic diagram of the RO test system. Pressure, flow, and sampling points are indicated.

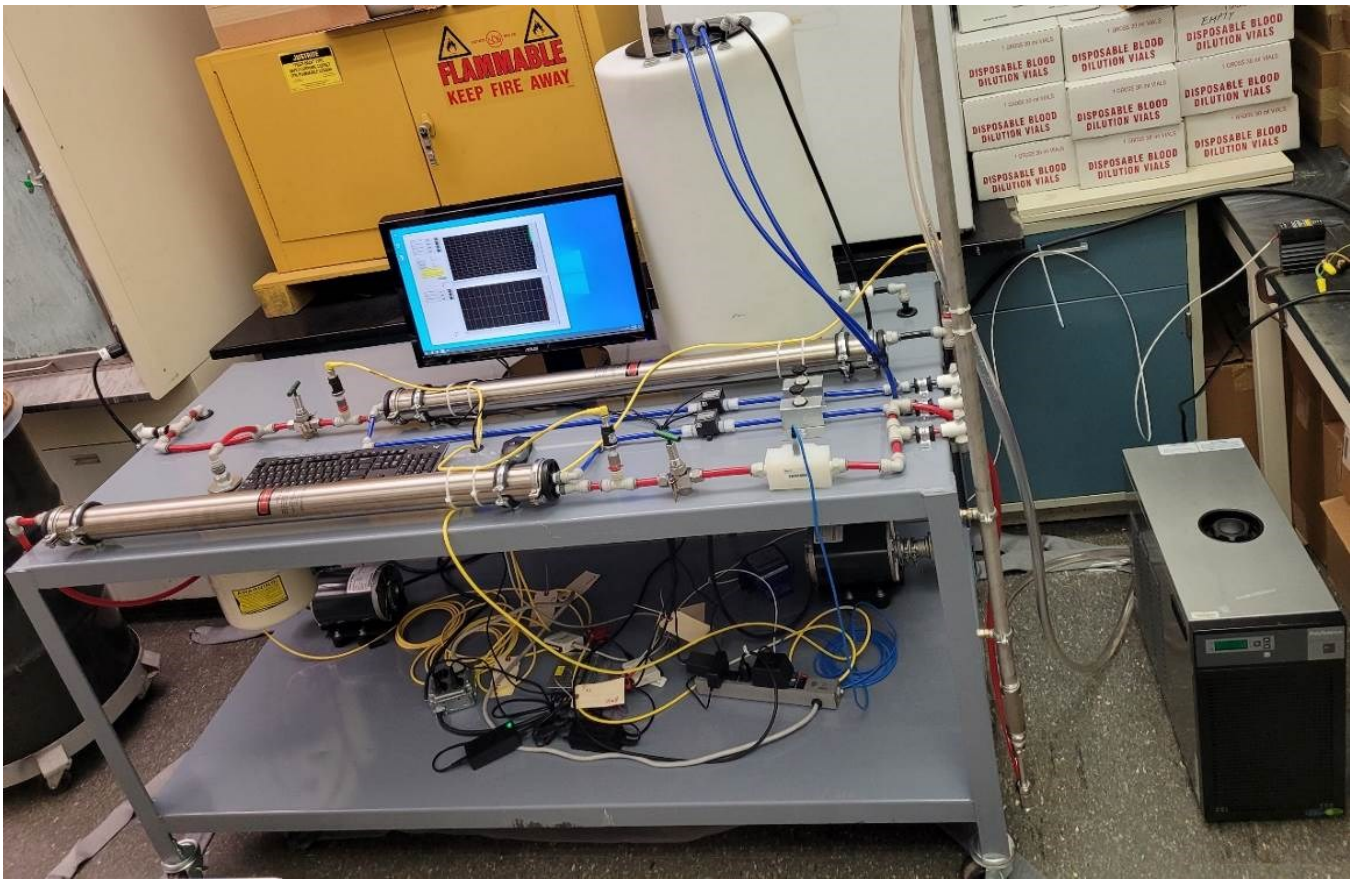

Figure 6.2. Photograph of the RO membrane test system.

Figure 6.3. Photograph of BW30-2540-43 RO element.

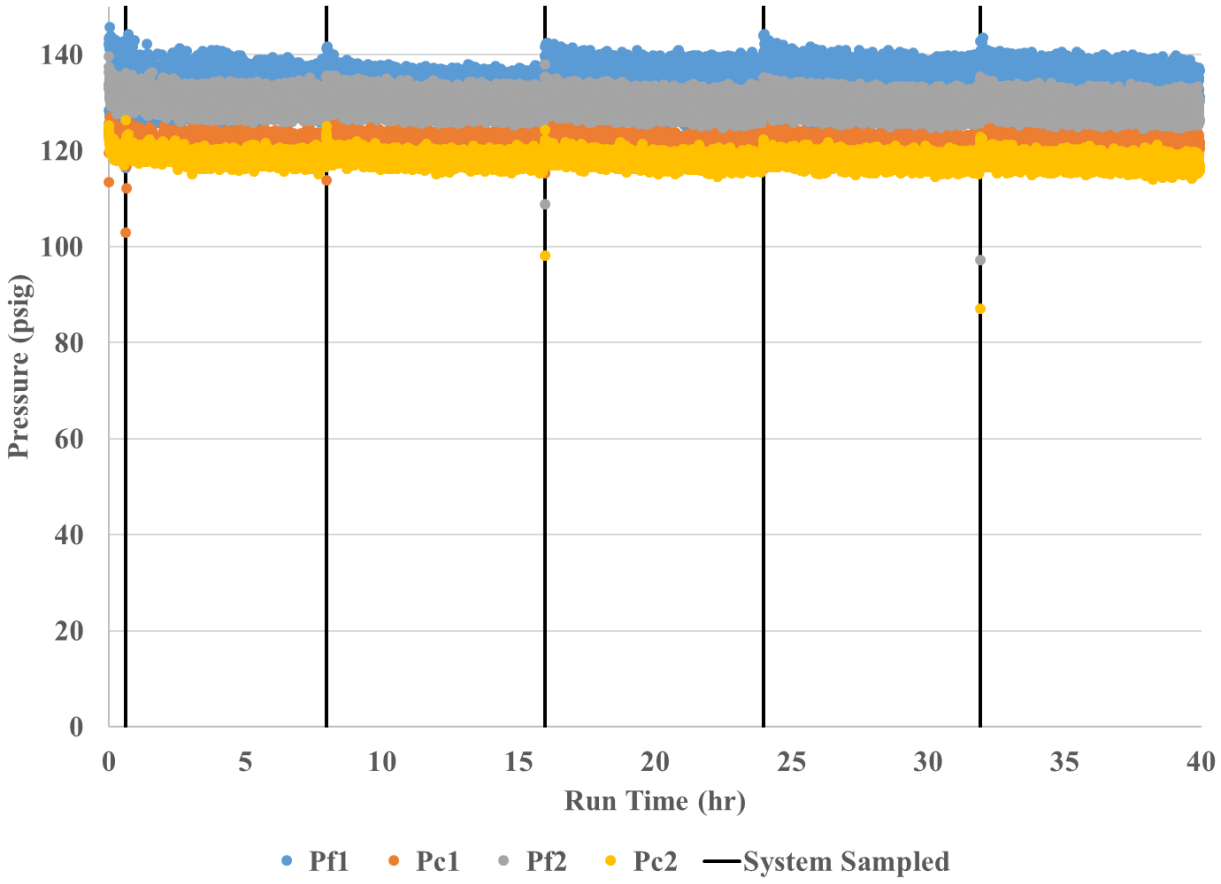

Figure 6.4. Process pressures during RO membrane testing. Membrane 1 inlet (Pf1), Membrane 1 outlet (Pc1), Membrane 2 inlet (Pf2), and Membrane 2 outlet (Pc2). The sample times are also indicated.

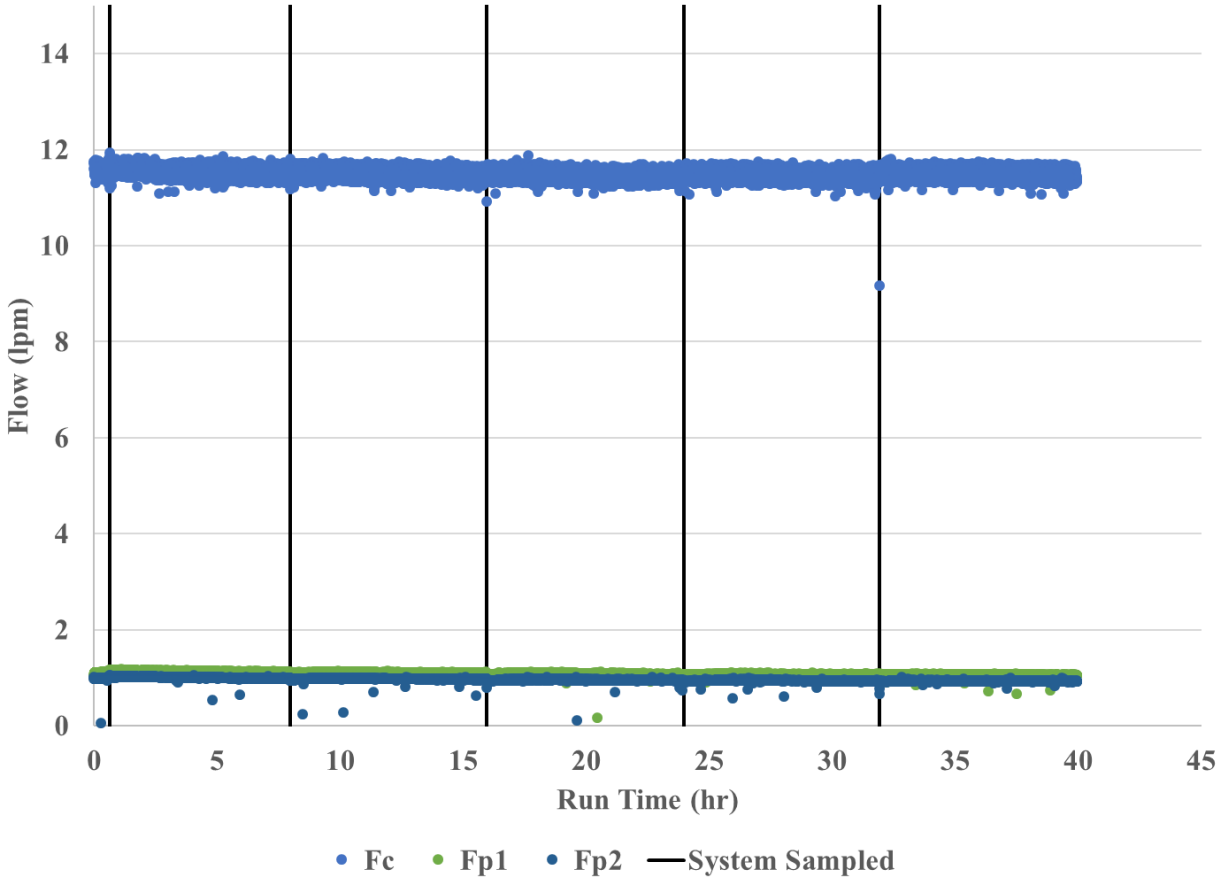

Figure 6.5. Process flow rates during RO membrane testing. Membrane 1 permeate (Fp1), Membrane 2 permeate (Fp2), and Membrane 2 concentrate (Fc). The sample times are also indicated.